

学位論文（要約）

Development of Wide Field and Broadband Cryogenic Optics with Microwave Kinetic Inductance Detectors

（マイクロ波力学的インダクタンス検出器用広視野・広帯域冷却光学系の開発）

平成 28 年 12 月 博士（理学）申請

東京大学大学院理学系研究科

天文学専攻

関口 繁之

Development of Wide Field and Broadband
Cryogenic Optics with Microwave Kinetic
Inductance Detectors

Shigeyuki Sekiguchi

Department of Astronomy, School of Science,
the University of Tokyo

December 2016

Acknowledgement

First of all, I would like to tell my sincere gratitude to all who gave me a kind advice and support.

I would like to express my gratitude to Prof. Yutaro Sekimoto for his enormous assistance and encouragement for five years. He gave me the best and the most interesting research theme, the development of wide FoV cryogenic optics and broadband corrugated horn. He was always around me and gave suitable tips for solving problems when I was saturated.

I would particularly like to thank Dr. Tom Nitta. He took care of me carefully and taught me a lot of things about a Microwave Kinetic Inductance Detector (MKID) and a optics when I was the 1st year of MA course. I also discussed about the wide FoV optics with him.

I learned a lot of things from Dr. Kenichi Karatsu. He was also kind enough to advise me on a measurement and analysis of the MKID.

It was my precious experience to discuss the development of OMT-MKID with Mr. Shibo Shu, Mr. Masakazu Sekine.

I appreciate all members of Mechanical Engineering Shop of National Astronomical Observatory of Japan. Especially, Mr. Norio Okada, Mr. Mitsuhiro Fukushima, and Mr. Kenji Mitsui kindly cared for me about the development of the cold optics, corrugated horn array and a lot of trivial components which are very important items for the experiment.

I feel grateful to Dr. Masahiro Sugimoto, Mr. Kouichi Kubo, and Mr. Toshikazu Takahashi about the development and evaluate of the corrugated horns. Especially, Dr. Masahiro Sugimoto gave me a lot of advice to develop of the corrugated horn array.

I would like to thank Prof. Takashi Noguchi and Prof. Hiroshi Matsuo for their lots of sincere advice.

Mr. Toshihiro Tsuzuki and Mr. Shingo Kashima gave me a great support and useful discussion on the design of wide FoV optics.

Dr. Dominjon Agnes, Dr. Takashi Hasebe and Mr. Takayuki Shimizu supported my experiment and discussed about the MKID.

Finally, I thank to my parents, brother and sister, and nephew and niece

ii

for their encouragement and continuous support for me at all times.

Abstract

Cosmic Microwave Background (CMB) radiation is a remnant about 380,000 years after the universe was born and it is described as a 2.73 K black body radiation. The temperature fluctuation has been precisely observed by WMAP and Planck satellites, and then cosmological parameters have been determined accurately. The inflation theory that an exponential expansion occurred in the early universe has been proposed to solve the horizon problem and the flatness problem. Since the CMB B-mode polarization is generated by inflationary gravitational waves, observing the B-mode leads to the verification of the inflation theory. The B-mode is expected to be noticeable in large angular scale, so a wide FoV millimeter-wave camera for surveying the whole sky is required.

In order to remove the foreground radiation, broadband observations in the 50 - 400 GHz band are also required. A multi-chroic detector which observes multiple frequency-bands in a pixel is effective in utilizing the limited focal plane. A broadband sensitivity of an octave or more is required for the feed of the detector.

Observations of submillimeter galaxies are important to elucidate diversity and evolution of galaxies. It is necessary to observe many submillimeter galaxies in order to understand the statistical property. A large field survey in the millimeter and submillimeter wave bands is needed for efficient observations. Therefore, a wide FoV instrument with a large single dish telescope is required.

In chapter 3, a cold optics anticipated the wide FoV millimeter and submillimeter wave observations using a large single dish telescope has been designed and developed. The requirements are 1. availability of a wide FoV observation with the modular optics, 2. a compact design using high refractive index and low loss lenses, 3. cooling down a superconducting detector temperature enough to get a high sensitivity of the detector, 4. reduction of the optical loading power.

The optics employs two high refractive lenses, high purity alumina ($n = 3.1$) and silicon ($n = 3.4$). We have developed for 220 GHz observations. It

is a compact cold re-imaging optics from a telescope focal plane with $F/\# = 6$ to a detector plane with $F/\# = 1$ at 100 mK. Since aluminum Microwave Kinetic Inductance Detectors (MKIDs) are installed, it is necessary to reduce the focal plane temperature below 150 mK. Three kinds of infrared (IR) blocking filters are used to prevent the incident power of the infrared coming from outside of a window. To get a high optical coupling efficiency of the detector, anti-reflection (AR) coating for the IR blocking filters and lenses is used. Therefore, the total transmittance of the three kinds of IR blocking filters is 0.78 at the observation frequency, and less than 10^{-10} above 6 THz. To reduce the incident stray light into the detector, a cold nested baffle composed of 4 reflectors with the same spherical shape has been developed. The stray light power is simulated to be $0.2 \mu\text{W}$ which corresponds a quarter of that of a without-baffles case. Thermal flow power into the detector, including the stray light power, is about $0.7 \mu\text{W}$. For a wider FoV observation, seven optical modules for the Antarctic 10 m terahertz telescope are designed.

In chapter 4, a broadband corrugated feed horn array has been developed. The geometry of corrugations is a plane structure so that the horn array can be directly machined from a bulk of aluminum with an end-mill. The cross-polarization and near side-lobe levels are less than -20 dB and -30 dB, respectively. The return loss is less than -15 dB in most design frequency bands, and the beam pattern is symmetric. The beam pattern and the return loss are measured in the 120 - 170 GHz range at room temperature. They are in good agreement with the simulation. It is possible to reduce reflection at the aperture surface and to reduce the weight by carving the unnecessary part.

A corrugated-horn coupled OMT - MKID camera has been demonstrated. The beam response of the horn-MKID was measured at 100 mK. Corrugated horn array modules for a large focal plane camera are designed for CMB B-mode observations.

Contents

1	Introduction	3
1.1	Cosmic Microwave Background	3
1.2	Submillimeter Galaxy	5
1.3	Superconducting detector	7
1.3.1	TES	7
1.3.2	MKID	8
1.4	Feed	8
1.4.1	Micro-lens	9
1.4.2	Corrugated horn array	9
1.5	Instruments for wide FoV observations	10
1.6	For broadband observations	15
2	Microwave Kinetic Inductance Detector	17
2.1	Principle of a Microwave Kinetic Inductance Detector	17
2.2	Shorted Quarter-wavelength Resonator	19
2.3	Capacitive Coupled Quarter-wavelength Resonator	22
2.4	Superconducting Microwave Resonator	23
2.5	Measurement System	26
2.6	Light Tight Setup	27
3	Wide Field Compact Cold Optics	33
3.1	Requirements	33
3.2	Design	36
3.2.1	Optical design	36
3.2.2	Mechanical design	39
3.2.3	Thermal design	39
3.2.3.1	IR blocking filter temperature	40
3.2.3.2	Non-anchored IR blocking filter temperature	40
3.2.3.3	Anchored IR blocking filter temperature	42
3.2.3.4	Thermal Calculation	46
3.2.3.5	Optical loading power	49

3.3	Components	51
3.3.1	IR blocking filters	51
3.3.2	Cold nested baffle	53
3.3.2.1	Design	53
3.3.2.2	Analysis	54
3.3.2.3	Fabrication	57
3.3.3	Lens holder	58
3.4	Cryogenic Experiment	61
3.5	Design of Wide FoV Cryogenic Optics for Antarctic 10-m Terahertz Telescope	61
4	Broadband Corrugated Feed Horn	67
4.1	Requirement	67
4.2	Design	68
4.3	Fabrication	74
4.4	Measurements	75
4.5	Discussion	78
4.6	Corrugated horn coupled multi-chroic MKID camera	82
4.6.1	Planar OMT antenna coupled MKID design	82
4.6.2	Cryogenic test with a wide FoV cold optics	84
4.6.2.1	Device holder design	84
4.6.2.2	Wide FoV cryogenic optics for horn coupled OMT-MKID	85
4.6.2.3	Hot/Cold response	86
4.6.2.4	Beam pattern measurement	86
4.6.2.5	Design for a large focal plane camera	88
5	Summary	91
	Bibliography	92

Chapter 1

Introduction

1.1 Cosmic Microwave Background

Cosmic Microwave Background (CMB) radiation, which was discovered by A. Penzias and R. Wilson in 1964 [2], is a remnant about 380,000 years after the universe was born. According to the standard cosmology, the universe was optically thick [3] because dense matter and radiation interacted with each other at high temperatures in the early universe. The temperature decreased with the expansion of the universe. When the temperature decreased about 3,000 K or less, the matter became neutral and decoupled with the radiation. Since then, the universe became optically thin or transparent, CMB is the oldest light that can be observed at the age of radiation decoupling. The spectrum of CMB is well described with blackbody radiation of 2.73 K with a peak at 150 GHz [4]. The temperature fluctuation of CMB observed by

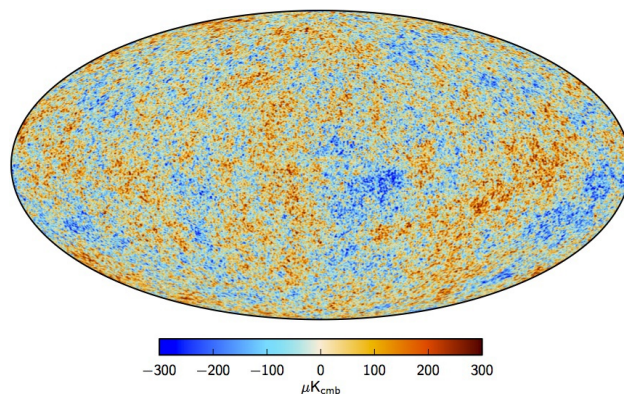


Figure 1.1: All-sky map of the CMB temperature fluctuation [1].

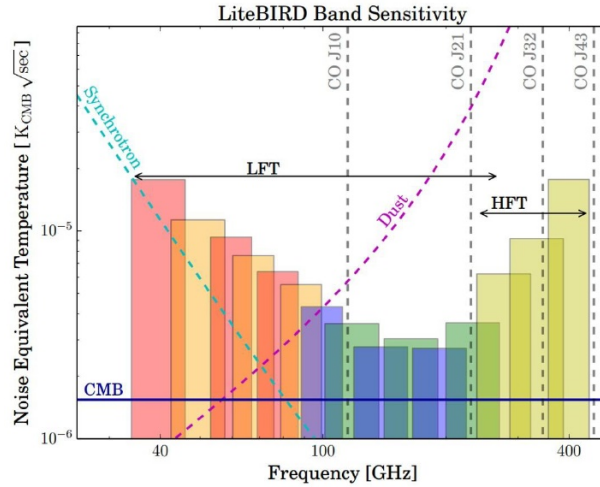


Figure 1.2: Frequency bands of the LiteBIRD satellite[7].

WMAP and PLANCK satellites has been precisely observed (Fig. 1.1), and then the age and cosmological parameters have been determined with high accuracy.

The CMB temperature is uniform with an accuracy of 10^{-5} . A fact that the background radiation coming from the other side of the universe has the same temperature indicates that the universe is uniform at least on the horizon scale. However, in the standard cosmology, since the horizon is smaller in the early universe, there should have been no causal relationship between distant points on the CMB, which is called as the horizon problem. In addition, the curvature of the present universe is very small, but to explain this, the density parameter of the initial universe must be equal to 1 with flatness of 10^{-15} (flatness problem). The inflation theory, that an exponential expansion occurred in the early universe, solves these problems [5, 6].

A clue to detect the cosmological inflation is the CMB polarization observations [8]. There are two modes of polarization pattern of CMB; one is E-mode with divergent pattern or parity symmetry and the other is B-mode with curl component or parity asymmetry [3].

The E-mode generated by Thomson scattering of photons has been detected by DASI [9]. The B-mode is generated by inflationary gravity wave during inflation [10, 11] or by the gravitational lens effect of the E-mode. Although the lensing B-mode has been observed by SPT-pol [12], the one derived from the inflation gravity wave has not been detected yet. Observing the CMB B-mode polarization leads to the verification of the inflation theory,

and it is possible to understand the early universe before the big bang [13, 8]. The B-mode derived from inflation gravity wave is much weaker signal than the E-mode and temperature fluctuation, so observation requires more sensitive detectors for polarization and wide field instruments for surveying the whole sky.

For accurate CMB polarization observations, it is necessary to separate the foreground radiation (see Fig. 1.2) of synchrotron and dust radiation from the galactic plane. So broadband observations in the 50 - 300 GHz band are also required. If one frequency band is assigned to a single pixel, the limited focal plane is divided by frequency bands to cover the broadband so the total number of detectors per band is reduced. Therefore, a multi-chroic pixel that detects multiple bands is important for effectively utilizing the limited focal plane. A broadband sensitivity of an octave or more is required for the feeds as well as the detectors.

A necessary time to get a CMB map sensitivity is derived as follows[14],

$$t_{\text{obs}} = \frac{\Omega \text{NET}^2}{\sqrt{C_{\ell}^{\text{noise}}}}, \quad (1.1)$$

where Ω is a solid angle, NET is a detector noise equivalent temperature, and C_{ℓ}^{noise} is an angular power spectrum of the CMB. If we observe the all-sky CMB using a single pixel of the Planck HFI receiver which has the NET of $57.5 (\mu\text{K s}^{1/2})$ at 149 GHz [15], 620 years are needed with an assumption; $\sqrt{C_{\ell}^{\text{noise}}} = 5(\mu\text{K arcmin})$. However, if we use 620 pixels at the frequency band, the time is reduced to one year. When we use a large pixel camera for the observation, the each pixel observes different point. Then, the observation using the large pixel camera is equivalent to the wide FoV one. Thus followings are required for CMB B-mode polarization observations.

1. Wide field cryogenic optics for an efficient survey of the whole sky.
2. Broadband feed and detector system

1.2 Submillimeter Galaxy

The shape and mass of galaxies in the neighboring universe vary widely, such as elliptical, spiral, bar and interacting or merging galaxies. Many mysteries remain in the diversity and evolution process of such galaxies. There are observations of distant submillimeter galaxies [16], [19] as a clue to elucidating the evolution of galaxies. Submillimeter galaxies are distant objects which are not observed in visible but in millimeter wave / submillimeter waves.

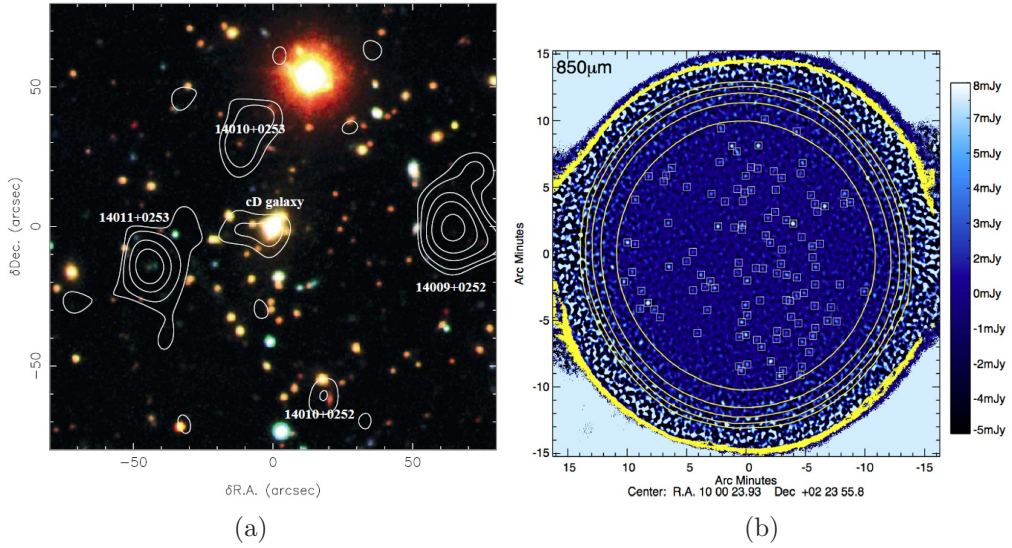


Figure 1.3: (a) A comparison of deep optical and submillimeter views of the sky [16]. The background color map is an optical image of the rich cluster of galaxies, overlaid with the white contours of a submillimeter-wave image. (b) The COSMOS 850 μm SCUBA-2 map [17].

They were detected by SCUBA on JCMT in 1998 [20]. Fig. 1.3 (a) is images of a visible and submillimeter wave (white contours) in the same area [16]. The intensity of the submillimeter wave does not correlate with that of the visible light. To understand their properties of submillimeter galaxies, it is required to observe many samples statistically, so a large field survey in the millimeter and submillimeter wave bands is necessary for efficient observations (see Fig. 1.3 (b) [17]). In recent years such large field surveys have been done by SPT[17], Herschel[21], and so on. Recent ALMA observations have captured the detailed structure of strong submillimeter galaxies found by SPT and have discovered many gravitational lensing objects (Fig. 1.4).

A plan to construct a 10-m terahertz survey telescope on Antarctica has been proposed by the University of Tsukuba [23]. In the Antarctica 10 m telescope, a large-scale survey is carried out with a multi-pixel superconducting camera. As shown in Fig. 1.5, optical depth in summer at the Dome Fuji of Antarctica is almost the same as that at Atacama plateau in winter[22]. The atmospheric transmittance in the winter season of Dome Fuji is expected to improve further, so it is an excellent site for submillimeter observations. The proposed Antarctica 10 m telescope, which is significantly larger than the Herschel dish size (3.5 m), will be essential to conduct deeper surveys at terahertz bands with a significantly smaller source confusion limit.

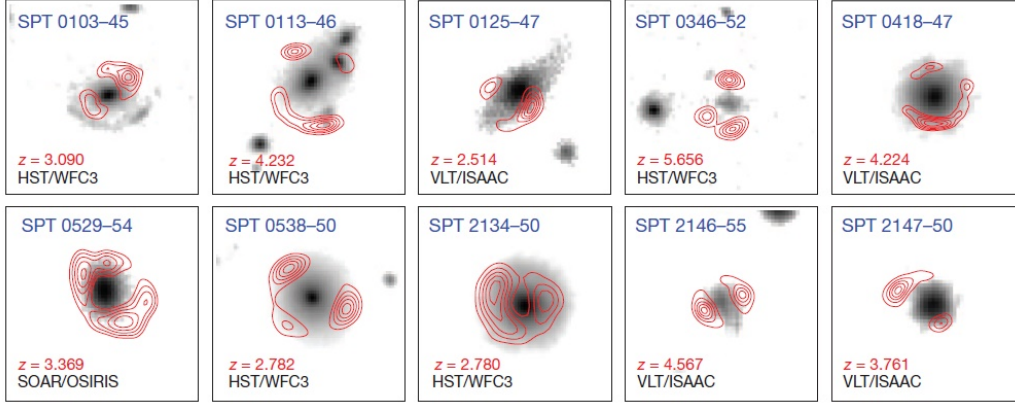


Figure 1.4: ALMA submillimeter wavelength (red contours) and near-infrared (grayscale) images of SPT targets[18].

Observing one square degree area using the 10 m telescope with 10,000 pixel detectors of 850 GHz requires 8 hours. It realizes faster mapping speed than that of SCUBA-2 of 670 GHz[24]. In comparison with 860 GHz band of Herschel[21], the 10 m telescope is valuable with the lower confusion limit and a large number of pixels.

1.3 Superconducting detector

1.3.1 TES

Bolometers based on semiconductors have been widely used for direct detectors [25]. The bolometer is a thermometer that converts electromagnetic energy of incident photons into thermal energy. Transition Edge Sensor (TES) [26, 27] is a bolometer made of a superconductor. Since the resistance of a superconductor changes abruptly with temperature near the critical temperature, it measures the energy of incident photons with high sensitivity. The sensitivity is expressed as the function of temperature; T and resistance; R , as follows,

$$\alpha \equiv \frac{d \ln R}{d \ln T} \quad (1.2)$$

and α is about two orders of magnitude larger than that of semiconductor bolometers. Moreover, by applying electrothermal feedback to TES, it is possible to maintain operating temperature around the critical temperature. For TES, it is necessary to bias for controlling the temperature of

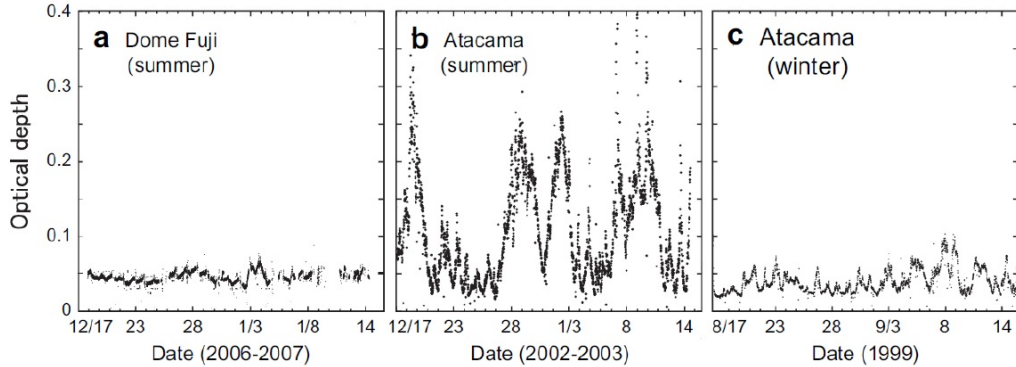


Figure 1.5: Optical depth between Dome Fuji and the Atacama ALMA site[22]. (a) Dome Fuji in summer, (b) Atacama in best summer, and (c) Atacama in best winter.

each element. The readout signals can be multiplexed with Superconducting Quantum Interference Devices (SQUID).

1.3.2 MKID

Microwave Kinetic Inductance Detector (MKID) is superconducting resonators operating at microwave frequencies [28]. Since the superconductor has a kinematic inductance L_k which varies with the number of Cooper pairs or quasi-particles, the resonant frequency of a superconductor is expressed as follows.

$$f_0 \propto \frac{1}{\sqrt{(L_g + L_k)C}} \quad (1.3)$$

where L_g is the geometrical inductance which does not depend on the number of Cooper pairs. When photons exceeding the gap energy of the superconductor are incident, the Cooper pairs of the superconductor film are broken into quasi-particles and the L_k changes. The incident energy is measured by the change of the resonance frequency.

We are developing MKIDs as a detector for the large field survey. Details of MKID are described in the next chapter.

1.4 Feed

Millimeter-wave detectors are generally used in combination with a transferring system called as “ feed ”, from quasi-optical modes to planar modes

on the detectors. The role of the feed is to collect signals and to define the beam pattern of the detector. Micro-lenses and corrugated horns are commonly used as a feed of millimeter-wave astronomical detectors.

1.4.1 Micro-lens

A combination of micro-lens and double slot planar antenna [29] has a capability of high-density feeds compared with corrugated horn due to high dielectric constant array of the lens. It means efficient use of the limited focal plane. In particular, by using a high dielectric such as silicon, the photon collecting capability increases and then it is possible to achieve high density integration of detectors [30].

There is a method of arranging hyper-spherical lenses on a substrate by adhesives [31]. In this case, the alignment of the planar antenna and the lens differs from element to element. Another method to fabricate micro-lens array is direct machining [32]. The spacing of the micro-lens array is determined by the fabrication machine, so the alignment can be made with higher accuracy, but the array size is limited by the machine workspace.

As the dielectric constant becomes higher, the reflectance on the surface becomes large, so the anti-reflection coating is crucial. Anti-reflection coating using epoxy resin has been reported [33, 31]. A broadband feed has been realized by combining the lenslet and sinuous antenna [34]. Meanwhile, as the lens becomes smaller, the beam pattern tends to have distortion. It also requires for preventing stray light to the lens array.

1.4.2 Corrugated horn array

Corrugated horns for millimeter-wave astronomy have been used with bandwidths less than $\sim 40\%$ [35, 36]. Ring-loaded corrugations have been designed to extend the bandwidth of a horn [37]. The ring load has a structure that expands the internal corrugation, which can be achieved with a platelet. A corrugated horn array with the Si MEMS platelets has been demonstrated to have an octave bandwidth [38].

Along with broader bandwidth of a corrugated horn, it is necessary to reduce the higher modes of the circular waveguide. A promising method of a four-probe orthomode transducer (OMT) with a 180 degree hybrid has been demonstrated [39]. To use the limited focal plane area efficiently, a broadband corrugated horn array with the planar OMT has been developed with incorporating frequency bandpass filters [40].

To cover a larger focal plane area corresponding to a wide field-of-view, it is desirable to manufacture a corrugated horn array with a reasonable

cost. Corrugated horns have been primarily manufactured by electroforming [41, 42]. Since it takes time and cost to fabricate them, it is not suitable for fabrication of the array. A corrugated horn assembled from split components directly machined from a bulk of aluminum has been demonstrated [43]. Recently, a corrugated horn (10 - 16 GHz) has been fabricated by using a 3D printer technology [44]. Because it is made of a plastic, it is not suitable for use in cryogenic temperature.

An array of feeds is essential to increasing mapping speed of astronomical observations (eg. [45]). Platelet or stacking of thin sheets with the thickness of a corrugation is an option to fabricate the array of corrugated horns [46]. A horn array fabricated by the platelet has been demonstrated to have a comparable performance with one by electroforming [47, 48]. Several groups have made the corrugated horn array by platelet or staking of the silicon or aluminum [49, 50, 51]. A smooth-wall horn array has been fabricated by direct machining (eg. [52]). The fractional bandwidth of this array is narrower than that of the corrugated horn.

1.5 Instruments for wide FoV observations

As mentioned before, wide field observations are essential for surveying the large sky for B-mode polarization observations and exploring high- z galaxies. Table. 1.1, 1.2, 1.3 summarize wide-field millimeter/submillimeter single-dish telescopes and instruments in the world.

It is indispensable to develop multi-pixel detectors to observe a wide field of view in millimeter/submillimeter waves. However, as the number of pixels of the diffraction limited optics increases, it is necessary to enlarge the available focal plane. In addition, for the high sensitivity of astronomical instruments, it requires to cool down the superconducting detectors at an extremely low temperature of ~ 0.1 K, so the heat capacity of the focal plane should be designed to be reasonably low. Therefore, it is important to design imaging optics with bright $F/\#$ feeds at the focal plane. Furthermore, to sufficiently cool down the detectors, the temperature of the optical system is gradually lowered. Appropriate low-pass filters are critical for reduction of infrared radiation to the detectors.

A wide-field optical system incorporating reflective mirrors becomes large as SCUBA-2 [53] and NIKA2 [54]. For future wider-field optics such as 30 m diameter with 1 degree FoV (eg. [55]), an optics covering the whole FoV with a modularized optical system is necessary. Since the focal plane of such a wide FoV telescope becomes larger, it is necessary to increase a vacuum window diameter of a cryostat. In order for a large vacuum window to

withstand atmospheric pressure, it is necessary to increase the thickness, which leads to loss of millimeter-wave signals. It is essential to develop a scalable and compact optics which is made of refractive optics using high dielectric constant lenses.

In the wide field optical system, the diameter of the vacuum window or the aperture becomes larger, so the contribution of incident stray light from outside the FoV to the detector is concerned. Counter-measures to prevent this stray light are indispensable for high precision observation.

In this thesis, we develop a wide field optical system to comply the following requirements.

1. Optics design which can be scaled as one module for wider FoV
2. Refractive optical system using high dielectric constant and low loss tangent material with anti-reflection coating
3. Cryogenics which the detector temperature cools down to 250 mK or less to operate superconducting detectors with high sensitivity
4. To reduce optical loading of the detectors from optical components and due to stray light

Table 1.1: Single dish telescopes for millimeter/submillimeter observation.

Telescope	Dish diameter	Frequency	Location	Altitude
NRO [56]	45 m	20 - 150 GHz	Nobeyama, Japan	1350 m
ASTE [57]	10 m	100 - 900 GHz	Atacama Desert, Northern Chile	4860 m
CSO [58]	10 m	150 - 860 GHz	Mauna Kea, Hawaii	4200 m
JCMT [59]	15 m	220 - 750 GHz	Mauna Kea, Hawaii	4092 m
IRAM [60]	30 m	150 - 500 GHz	Pico Veleta, Spain	2870 m
LMT [61]	50 m	75 - 350 GHz	Sierra Negra, México	4600 m
ACT [62, 63]	6 m	150 - 280 GHz	Atacama Desert, Northern Chile	5200 m
SPT [64]	10 m	95 - 345 GHz	South Pole, Antarctica	2800 m
HTT [65]	3.5 m	150 GHz	Atacama Desert, Northern Chile	5190 m

Table 1.2: Instruments for CMB observations

	POLARBEAR[66], [65]	BICEP[67], [68]	BICEP2[69]	SPTpol[70, 64]	ACTpol[71, 63]
Telescope	HTT	BICEP	BICEP2	SPT	ACT
Frequency (GHz)	148	100 / 150	150	90 / 150	97 / 148
Window	Zotefoam	Zotefoam	Zotefoam	Zotefoam	UHMWPE
Window Size (mm)	300	300	320	300	340
IR Filter	metal mesh porous PTFE	metal mesh PTFE	metal mesh PTFE, nylon	metal mesh	metal mesh
Optics	refractive	refractive	refractive	hybrid	refractive
Lens	HDPE	HDPE	HDPE	HDPE	silicon
Number of Lens	3	2	2	1	3×3
Focal Plane Dia. (mm)	190	250 (@ 4 K)	250	150	150×3
Focal Plane Temp. (mK)	250	250	250	280	100
Feed Type	lens	corrugated horn	phased array	corrugated horn	corrugated horn
Detector	TES	PSB	TES	TES	TES
No. of Detectors	1274 (637 pixel)	98 (49 pixel)	512 (256 pixel)	1536 (768 pixel)	3068 (1534 pixel)

Table 1.3: Instruments for millimeter astronomy

	SCUBA-2[53]	NIKA2[54]	MUSIC [72, 73, 74]
Telescope	JCMT	IRAM	CSO
Frequency (GHz)	350 / 670	150 / 260	150 / 220 / 300 / 350
Window	Polyethylene		HDPE
Window Size (mm)	180	~ 400	300
IR Filter	metal mesh	metal mesh	metal mesh
Optics	reflective	hybrid	refractive
Lens		HDPE	UHMWPE
Number of Lens	0	6	1
Focal Plane Dia. (mm)	120	80	130
Focal Plane Temp. (mK)	100	150	240
Feed Type	absorber	absorber	phased array
Detector	TES	LEKID	MKID
No. of Detectors	10000	2240	2304 (576 pixel)

1.6 For broadband observations

As described in the previous section, broad bandwidth of the cryogenic optical system is important for effectively utilizing the limited focal plane. When a refractive optical system is used for a wide field optical system, millimeter waves are reflected at the surface due to a change of the refractive index. As the refractive index becomes higher, the reflection increases, which causes loss of signals and non-linear standing-wave effects. Anti-reflection coating on the lens is required to reduce them. Epoxy resins and sub-wavelength structures have been reported as the anti-reflection coatings [33]. Multi-layered anti-reflection coatings have been proposed to make them broader bandwidth [31, 75].

A corrugated horn has excellent properties for polarization measurements such as a symmetrical beam, low side-lobe, and low cross-polarization. However, the bandwidth had been limited to 1:1.4 [76]. So broad bandwidth of corrugated horn is a challenging item. A corrugated horn with a ring-load structure has been designed to have an octave bandwidth [37]. It has been manufactured by Si micro-machined platelets [38]. However, the weight of the platelet corrugated horn is limited by fixture bolts for stacking tightly. Since many corrugated horn arrays are arranged on the focal plane to cover a wide FoV, light weight of the horn array is desirable, especially for space applications. Therefore, in this thesis, we have developed a feed for following requirements.

1. Broadband corrugated horn array
2. Light weight feeds
3. Easy fabrication of feeds for a number of the horn-array modules

Chapter 2

Microwave Kinetic Inductance Detector

2.1 Principle of a Microwave Kinetic Inductance Detector

Microwave Kinetic Inductance Detector (MKID) [28] consists of superconducting resonators with coplanar waveguide (CPW) geometry which are capacitively coupled to a CPW feed line. A couple of coaxial cables is available to readout 1000 pixel MKIDs using frequency domain multiplexing [77]. Then, the thermal flow into the detector via the cables becomes less than the other superconducting detectors such as TES and STJ. It is an advantage of MKID to realize a large-format pixel camera. In this thesis, MKID is used as a detector of a camera.

According to the BCS theory [78], there is an indirect attractive interaction between two electrons via phonon in a superconductor. The bound electrons are called a Cooper pair and the mean distance between the electrons is around the Pippard's coherence length [79].

The binding energy of the Cooper pair is

$$E_{gap} = 2\Delta(T), \quad (2.1)$$

where $\Delta(T)$ is a gap energy of superconductor and when a temperature is less than a half of the critical temperature; T_c , the gap energy is written as follows,

$$2\Delta(T) \approx 2\Delta(0) = 3.52k_B T_c, \quad (2.2)$$

and when $T \sim T_c$, $\Delta(T)$ depends on a temperature as follows and see Fig.2.1,

$$\Delta(T) \simeq 3.2k_B T_c \left(1 - \frac{T}{T_c}\right)^{1/2}. \quad (2.3)$$

When a photon having an energy over E_{gap} enters a superconductor, a Cooper pair is broken and two quasi particles are generated (Fig. 2.2).

MKID is a superconducting resonator operated in microwave range. The equivalent circuit consists of a parallel resonance circuit with capacitively coupled to a feed line, as shown in Fig.2.3. The resonant frequency; f_0 is

$$f_0 = \frac{1}{4l\sqrt{(L_g + L_k)C}}. \quad (2.4)$$

Where, l is a length of resonator and L_g , L_k , and C are geometry inductance, kinetic inductance, and capacity per unit length, respectively. L_g is defined by a geometry of MKID and doesn't depend on an incident photon. L_k depends on the number of quasi particles. Since incident photons break Cooper pairs and that leads to a change of the L_k , the resonant frequency is changed as follow;

$$f'_0 = f_0 + \Delta f = \frac{1}{4l\sqrt{(L_g + L_k + \Delta L_k)C}}. \quad (2.5)$$

Then, the incident photon energy is calculated by the difference of the read-out signal.

A part which inputs a photon signal to an MKID is necessary since an MKID responses to all photon whose energy is higher than E_{gap} . Therefore, according to coupling a designed antenna depending on observation frequency

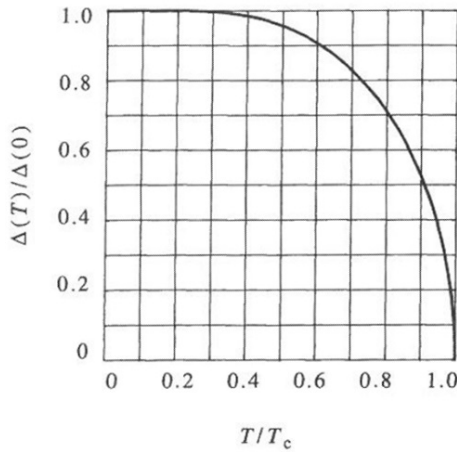


Figure 2.1: Temperature dependence of a gap energy[79]

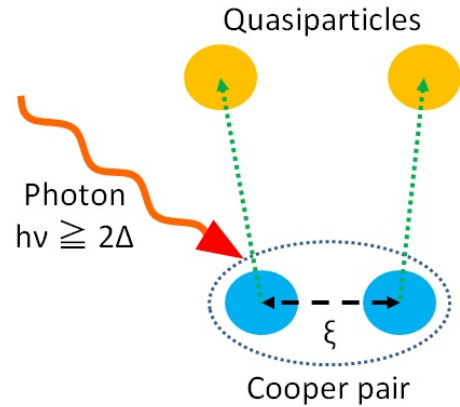


Figure 2.2: Generations of quasi particles.

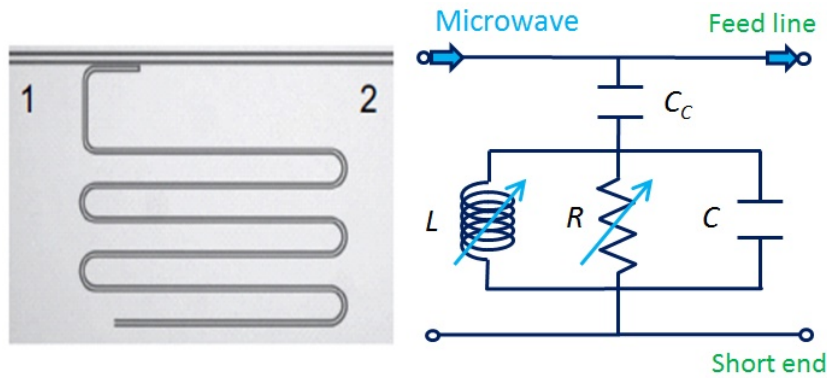


Figure 2.3: Equivalent circuit of an MKID

to the short side edge of the MKID, the MKID has a response at the designed frequency.

2.2 Shorted Quarter-wavelength Resonator

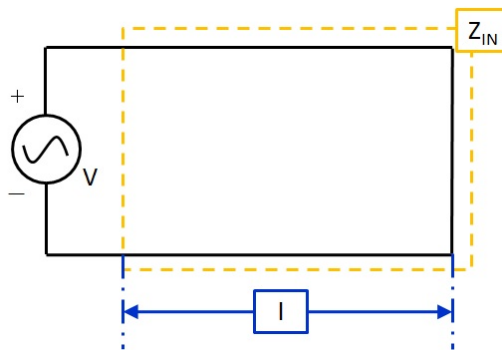


Figure 2.4: Shorted quarter-wavelength resonator

In this section, we expound a resonator consisted with transmittance line [80] since MKID is a microwave resonator. The input impedance of a transmission line with the length of l (Fig. 2.4) is

$$\begin{aligned}
Z_{\text{in}} &= Z_0 \tanh(\alpha + j\beta)l \\
&= Z_0 \frac{\tanh(\alpha l) + \tanh(j\beta l)}{1 + \tanh(\alpha l) \tanh(j\beta l)} \\
&= Z_0 \frac{1 - j \tanh(\alpha l) \cot(\beta l)}{\tanh(\alpha l) - j \cot(\beta l)}, \tag{2.6}
\end{aligned}$$

where Z_0 , α , and β are characteristic impedance, attenuation constant, and phase constant, respectively. The length of the line is $l = \lambda/4$ with $\lambda = 2\pi v_p/\omega_0$, (v_p : phase velocity). A near frequency of the resonance is $\omega = \omega_0 + \Delta\omega$, and because of the relationship; $\beta = \omega/v_p$,

$$\beta l = \frac{(\omega_0 + \Delta\omega)l}{v_p} = \frac{\pi}{2} + \frac{\pi\Delta\omega}{2\omega_0}, \tag{2.7}$$

and

$$\cot(\beta l) \approx -\frac{\pi\Delta\omega}{2\omega_0} \quad (\Delta\omega \ll \omega_0). \tag{2.8}$$

Here, the transmission line is assumed low loss; ($\alpha \ll 1$),

$$\tanh(\alpha l) \approx \alpha l. \tag{2.9}$$

According to the equations; eqs.(2.6), (2.8), and (2.9), the characteristic impedance is written,

$$Z_{\text{in}} = Z_0 \frac{1 + j\alpha l \frac{\pi\Delta\omega}{2\omega_0}}{\alpha l + j \frac{\pi\Delta\omega}{2\omega_0}} \approx \frac{Z_0}{\alpha l + j\pi\Delta\omega/2\omega_0}. \tag{2.10}$$

On the other hand, an impedance in a near frequency of the resonance of an RLC parallel resonator is written using the relationship; $\omega_0 = 1/\sqrt{LC}$,

$$\begin{aligned}
Z_{\text{in}} &= \left\{ \frac{1}{R} + j(\omega_0 + \Delta\omega)C + \frac{1}{j(\omega_0 + \Delta\omega)L} \right\}^{-1} \\
&\approx \frac{1}{(1/R) + 2j\Delta\omega C}. \tag{2.11}
\end{aligned}$$

Comparison with the input impedance of a quarter-wavelength transmission line(eq.(2.10)) suggests that the resistance, capacitance, and inductance of the equivalent RLC circuit of the transmission line are,

$$R = \frac{Z_0}{\alpha l} \tag{2.12}$$

$$C = \frac{\pi}{4\omega_0 Z_0} \tag{2.13}$$

$$L = \frac{1}{\omega_0^2 C}. \tag{2.14}$$

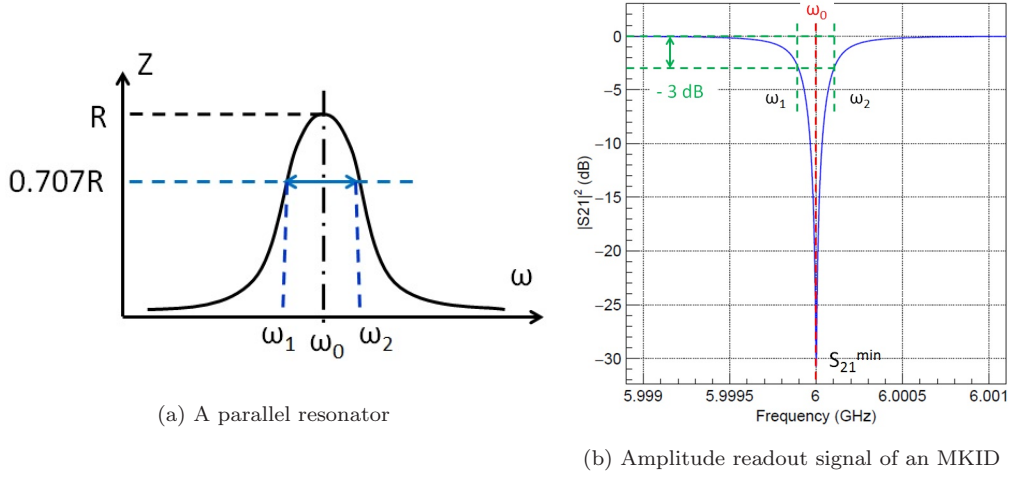


Figure 2.5: Spectra of resonators.

A quality factor which shows a sharpness of the resonance is defined as,

$$Q = \omega_0 \frac{\text{average energy stored}}{\text{energy loss/second}} \quad (2.15)$$

Then, a Q of a quarter-wavelength resonator is,

$$Q = \omega_0 RC = \frac{\pi}{4\alpha l} = \frac{\beta}{2\alpha}, \quad (2.16)$$

where $l = \pi/2\beta$. Using the eq.(2.10), the impedance of a shorted quarter-wavelength resonator is

$$Z_{\text{in}} = \frac{4Z_0Q/\pi}{1 + 2jQ\Delta\omega/\omega_0} = \frac{4Z_0Q/\pi - \frac{8jZ_0Q^2}{\pi} \frac{\Delta\omega}{\omega_0}}{1 + 4Q^2(\Delta\omega/\omega_0)^2}. \quad (2.17)$$

A relationship of the Q and FWHM; $\Delta\omega$ is as follows,

$$Q = \frac{\omega_0}{\Delta\omega(\text{FWHM})} = \frac{\omega_0}{\omega_2 - \omega_1}. \quad (2.18)$$

Where, ω_1 and ω_2 are the frequencies whose amplitude becomes half power of resonance ($\omega_2 > \omega_1$). From eq.(2.18), the Q is derived from the spectrum of a resonator.

2.3 Capacitive Coupled Quarter-wavelength Resonator

A capacitive coupled shorted quarter-wavelength resonator is described in [81]. This resonator is the same as MKID we used in this thesis.

According to adding the coupler to the quarter-wavelength resonator, the total quality factor: Q_l is redefined,

$$\frac{1}{Q_l} = \frac{1}{Q_i} + \frac{1}{Q_c}. \quad (2.19)$$

Where Q_i and Q_c are quality factors of a shorted quarter-wavelength resonator and a coupler, respectively. Q_c is derived from the definition of quality factor, eq.(2.15),

$$Q_c = \frac{\pi}{2Z_0^2(\omega_0 C_c)^2}. \quad (2.20)$$

The impedance is also redefined, as follows.

$$Z = \frac{-j}{\omega C_c} + \frac{4Z_0 Q_i / \pi - \frac{8jZ_0 Q_i^2}{\pi} \frac{\Delta\omega}{\omega_{1/4}}}{1 + 4Q_i^2 (\Delta\omega / \omega_{1/4})^2}. \quad (2.21)$$

The resonance frequency of shorted quarter-wavelength resonator is changed to $\omega_{1/4}$. The resonance occurs at a frequency $\omega_0 < \omega_{1/4}$, where $\text{Im}(Z) = 0$. When $\text{Im}(Z) = 0$, the solution of eq.(2.21) has two frequencies. However, $\text{Re}(Z)$ of the higher one which is closer the $\omega_{1/4}$ becomes larger and doesn't load the through line. Then, by selecting another frequency as the resonance one, ω_0 is

$$\Delta\omega = \omega_0 - \omega_{1/4} \approx -\frac{2Z_0 C \omega_0 \omega_{1/4}}{\pi} \approx -\frac{2Z_0 C \omega_{1/4}^2}{\pi}. \quad (2.22)$$

Where, the loss in the transmission line is assumed enough low, and ω_0 is close to $\omega_{1/4}$. According to eq.(2.20),(2.21), and (2.22), the impedance close to ω_0 is,

$$\begin{aligned} Z &= \frac{\pi}{4Z_0(\omega_0 C_c)^2 Q_i} \left(1 + \frac{2jQ_i \Delta\omega'}{\omega_0} \right) \\ &= Z_0 \frac{Q_c}{2Q_i} (1 + 2jQ_i \delta x). \end{aligned} \quad (2.23)$$

Here, $\delta x = \Delta\omega' / \omega_0$, $\Delta\omega' = \omega - \omega_0$.

The transmittance value of a scattering matrix, S_{21} is utilized to measure the MKID signals. S_{21} is defined as the voltage ratio of transmitting wave from input port 1 to output port 2 (see, Fig. 2.3),

$$S_{21} = \frac{2Y_0}{2Y_0 + Y} = \frac{2}{2 + \frac{Z_0}{Z}}, \quad (2.24)$$

$Y = 1/Z$ is called as admittance. Then, S_{21} at the resonance frequency $\delta x = 0$ of the capacitive coupled shorted quarter-wavelength resonator is

$$S_{21}^{\min} = \frac{Q_c}{Q_c + Q_i}, \quad (2.25)$$

and close to the resonance frequency $\delta x \ll 1$ is

$$S_{21} = \frac{S_{21}^{\min} + 2iQ_l\delta x}{1 + 2iQ_l\delta x}. \quad (2.26)$$

Where Q_l is a total quality factor of the resonator and $Q_l = Q_i Q_c / (Q_i + Q_c)$. S_{21} signal of a resonator which has $Q_i = 1 \times 10^6$, $Q_c = 1 \times 10^5$, $f_0 = 6\text{GHz}$, is plotted in Fig. 2.6, and it becomes a circle with the center point $x_c = (1 + S_{21}^{\min})/2$. The amplitude: A and phase: θ of the resonator are defined using this circle, as follows,

$$A = \sqrt{(\text{Re}|S_{21}| - x_c)^2 + \text{Im}|S_{21}|^2}. \quad (2.27)$$

$$\theta = \arctan\left(\frac{\text{Im}|S_{21}|}{\text{Re}|S_{21}| - x_c}\right). \quad (2.28)$$

They are shown in Fig. 2.7.

2.4 Superconducting Microwave Resonator

In this section, we expound the MKID behavior as a superconductor.

Kamerlingh - Onnes discovered the vanishing of the electrical resistance of the superconductor below the critical temperature. In 1932, the changing of the electrical conductivity was confirmed at radio frequency (1 - 10 MHz) [82], [83]. This is because the conductivity in a superconductor is written as a complex number,

$$\sigma(\omega) = \sigma_1(\omega) - j\sigma_2(\omega), \quad (2.29)$$

where σ_1 and σ_2 are described by Mattis - Bardeen [84].

$$\frac{\sigma_1(\omega)}{\sigma_n} = \frac{2}{\hbar\omega} \int_{\Delta}^{\infty} dE \frac{E^2 + \Delta^2 + \hbar\omega E}{\sqrt{E^2 - \Delta^2} \sqrt{(E + \hbar\omega)^2 - \Delta^2}} [f(E) - f(E + \hbar\omega)] \quad (2.30)$$

$$\frac{\sigma_2(\omega)}{\sigma_n} = \frac{2}{\hbar\omega} \int_{\Delta}^{\Delta} dE \frac{E^2 + \Delta^2 - \hbar\omega E}{\sqrt{E^2 - \Delta^2} \sqrt{\Delta^2 - (E - \hbar\omega)^2}} [1 - 2f(E)] \quad (2.31)$$

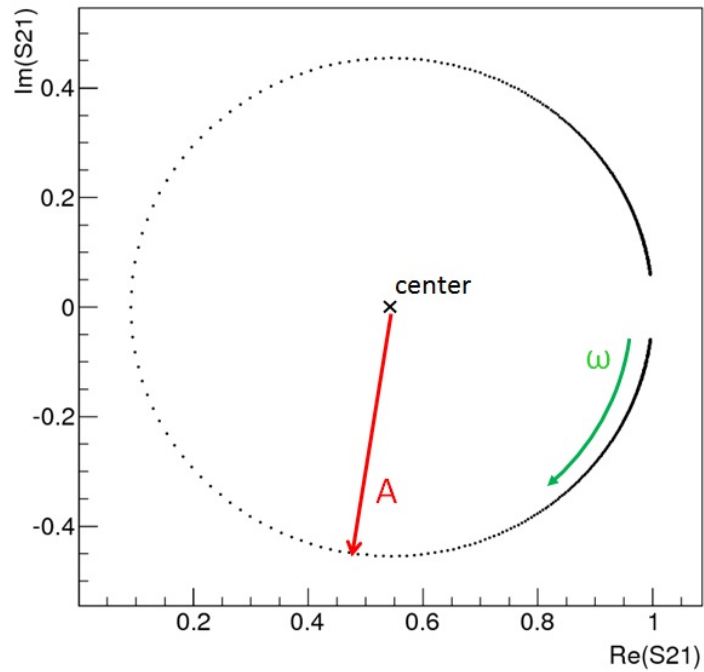


Figure 2.6: S_{21} signal in the complex plane of a capacitive coupled quarter-wavelength resonator near the resonance frequency.

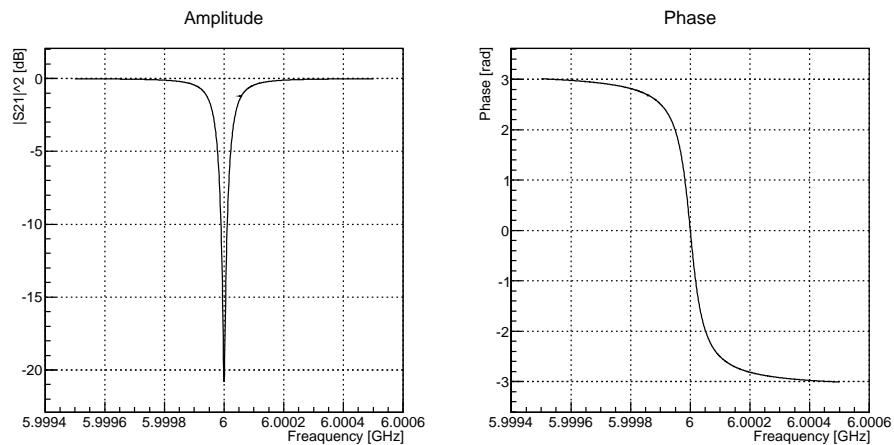


Figure 2.7: The amplitude and phase of a capacitive coupled quarter-wavelength resonator near the resonance frequency.

$f(E)$ is the distribution function for unpaired normal electrons or quasiparticles, and in the case of thermal equilibrium is given by the Fermi-Dirac distribution $f(E) = 1/(e^{E/k_B T} + 1)$. The quasiparticle density is given[85],

$$n_{qp} = 4N_0 \int_{\Delta}^{\infty} dE \frac{E^2}{\sqrt{E^2 - \Delta^2}} f(E) \simeq 2N_0 \sqrt{2\pi k_B T \Delta(0)} \exp\left(\frac{-\Delta(0)}{k_B T}\right), \quad (2.32)$$

where N_0 is the single-spin density of electron states at the Fermi energy. At low temperature ($T \ll T_c$), σ_1 and $\delta\sigma_2(\omega, T) = \sigma_2(\omega, T) - \sigma_2(\omega, 0)$ are proportional to n_{qp} [77], so the variation of the quasiparticle density is regarded as that of the complex conductivity. The complex conductivity makes an effect on a surface inductance, L_s and a quality factor of superconductor [86],

$$\frac{\delta L_s}{L_s} = -\frac{\beta}{2} \frac{\delta\sigma_2}{\sigma_2} \quad (2.33)$$

$$\frac{\delta Q}{Q} = -\left(\frac{\delta\sigma_1}{\sigma_1} - \frac{\delta\sigma_2}{\sigma_2}\right) \quad (2.34)$$

$$\beta = 1 + \frac{2d/\lambda}{\sinh(2d/\lambda)}. \quad (2.35)$$

Where, d is the thickness of the superconductor and λ is the magnetic penetration depth. Using eqs.(2.4) and (2.33), a variation in the kinetic inductance and complex conductivity change the resonant frequency,

$$\frac{\delta\omega_0}{\omega_0} = -\frac{\alpha_k}{2} \frac{\delta\omega_0}{\omega_0} = \frac{\alpha_k \beta}{4} \frac{\delta\sigma_2}{\sigma_2}. \quad (2.36)$$

Where α_k is a kinetic fraction defined as, $\alpha_k = \frac{L_k}{L_k + L_g}$. When only the complex conductivity is concerned, the amplitude and phase of MKID become,

$$A = 1 - 2\frac{Q_l}{Q_i} \left(\frac{\delta\sigma_1}{\sigma_1} - \frac{\delta\sigma_2}{\sigma_2}\right) \quad (2.37)$$

$$\theta = -\alpha_k \beta Q_l \frac{\delta\sigma_2}{\sigma_2}. \quad (2.38)$$

The amplitude and phase sensitivity to the quasiparticle density of the resonator is written [81],

$$\frac{dA}{dN_{qp}} = -\frac{\alpha_k \beta Q}{|\sigma| V} \frac{d\sigma_1}{dn_{qp}} \quad (2.39)$$

$$\frac{d\theta}{dN_{qp}} = -\frac{\alpha_k \beta Q}{|\sigma| V} \frac{d\sigma_2}{dn_{qp}}. \quad (2.40)$$

In a low temperature case ($T \ll T_c$), $|\sigma| \approx \sigma_2$.

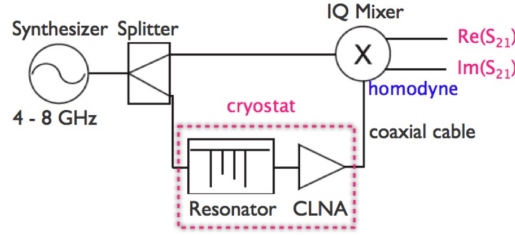


Figure 2.8: A measurement system of an MKID

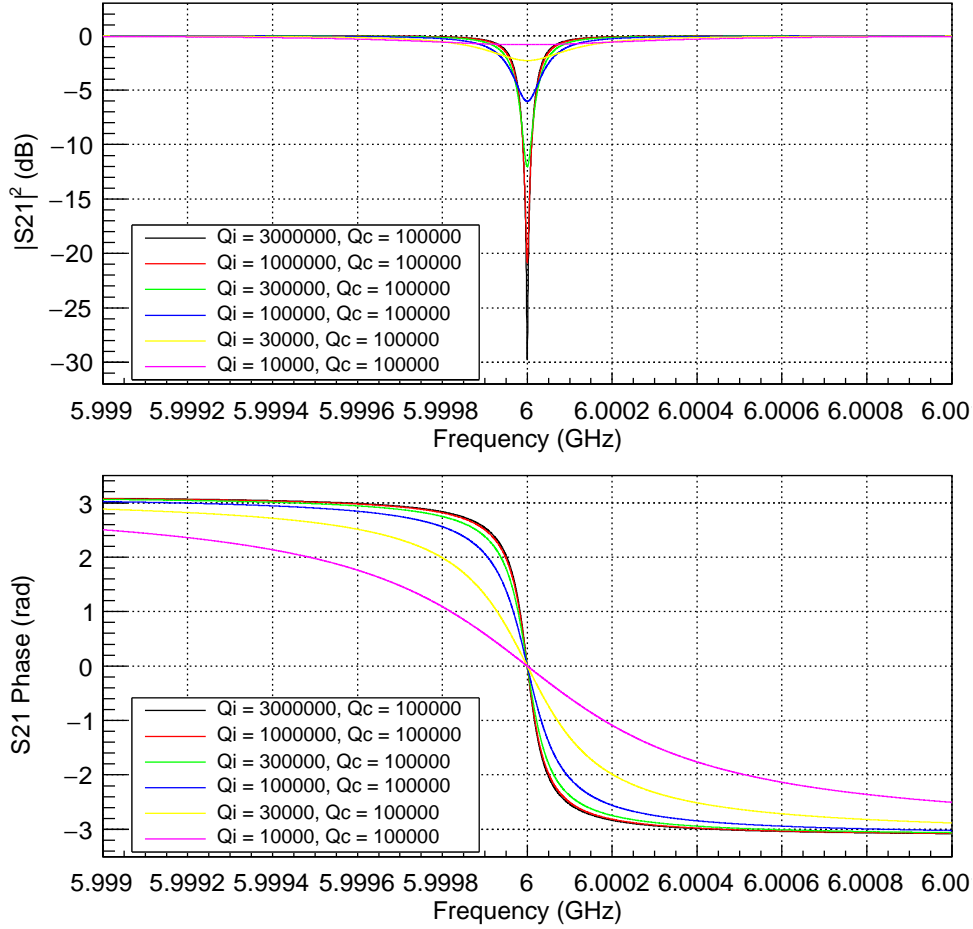
2.5 Measurement System

A schematic measurement system of an MKID is shown in Fig. 2.8. The signal generator provides the microwave signal, which is split into two parts; one goes to the MKID in a cryostat and the other goes to an IQ mixer as the LO signal. After transmitting the MKID, the signal is amplified and goes to the IQ mixer as the RF signal. Then, IQ mixer outputs the real and imaginary parts of the S_{21} signal, respectively, which are plotted in a Fig. 2.6 on an IQ plane.

In eq.(2.26), the S_{21} signal depends on the quality factor, Q . The Q_i dependence of amplitude and phase are shown in Fig. 2.9 when $Q_c = 1 \times 10^5$, $f_0 = 6$ GHz with variations of $Q_i = 1 \times 10^4, 3 \times 10^4, 1 \times 10^5, 3 \times 10^5, 1 \times 10^6, 3 \times 10^6$. Q_c dependence of amplitude and phase are also shown in Fig.2.10. When Q_i becomes higher and higher, the depth of the amplitude dip does deeper and the phase also changes drastically around the resonant frequency. On the other hand, When Q_c becomes higher, the phase changes drastically, but the dip of the amplitude becomes shallow. However, a low Q_c generates the deep amplitude with large FWHM and Q_l becomes low.

When incident photons break the Cooper pairs, the S_{21} signal is changed as shown in Fig. 2.11. Since the incident photon energy is determined by the variance of the δA and $\delta\theta$, the high Q MKID has high sensitivity. The high Q_l resonance with small FWHM is available to multiplex the resonant frequencies with close interval.

One of the advantages of the MKID is a readout signal multiplexing. A superconducting detector is used at below 1 K, so the number of readout cables, which transfer the thermal flow between the detector and the room temperature part, is required to be small. The signal multiplexing is a technique which leads the information of the multi detector signal with one cable. The technique is necessary to make a large pixel camera. There are three ways of multiplexing technique, Time Domain Multiplexing (TDM), Frequency

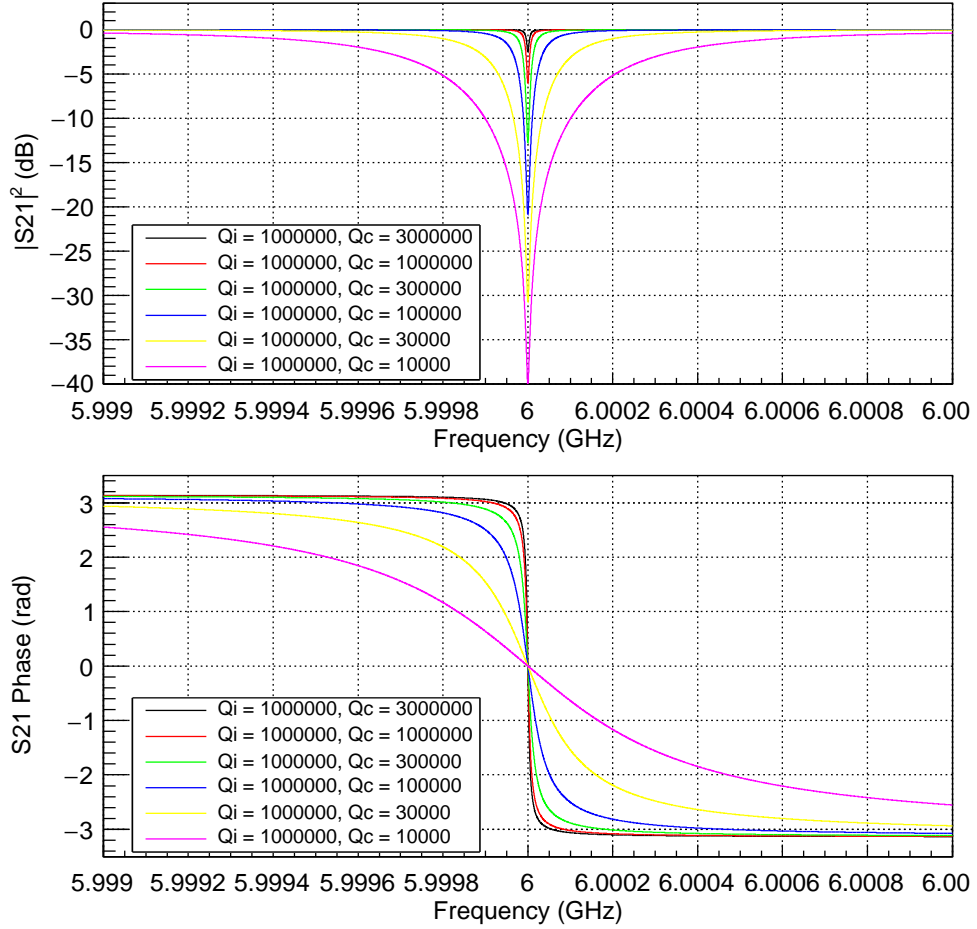
Figure 2.9: Q_i dependence of amplitude and phase.

Domain Multiplexing (FDM) and Code Division Multiplexing (CDM).

MKID utilizes the FDM. The resonant frequency of the MKID is expressed in eq.(2.4), and the resonant frequency of each pixel is designed with length of resonator l . MKID array is realized by coupling all resonators to a feed line and setting the resonant frequencies by changing the l slightly. It is possible to multiplex 1000 to 10000 resonances with a couple of cables.

2.6 Light Tight Setup

In order to increase the sensitivity of MKID, it is necessary to get large quality factors. Noise Equivalent Power (NEP) is utilized as a barometer of

Figure 2.10: Q_c dependence of amplitude and phase.

a detector sensitivity. The electrical NEP of an MKID using phase readout and amplitude readout is described in [81, 87],

$$NEP^2(\omega) = S_x(\omega) \left(\frac{\eta \tau_{qp}}{\Delta} \frac{\partial x}{\partial N_{qp}} \right)^{-2} (1 + \omega^2 \tau_{qp}^2)(1 + \omega^2 \tau_{res}^2), \quad (2.41)$$

where x is θ for phase readout or R for amplitude readout. Here S_θ is the phase noise in rad^2/Hz , S_R the amplitude noise in $1/\text{Hz}$, N_{qp} the total number of quasiparticles, Δ the energy gap of the superconductor, τ the quasiparticle lifetime, τ_{res} the resonator ring time, and $\eta = 0.57$ the efficiency of quasiparticle creation. Since MKID has two kinds of readout data; amplitude and phase, the two kinds of NEPs derived amplitude and phase are exist; NEP_{Amp} and NEP_{pha} . NEP_{pha} doesn't depend on the quality factor and is

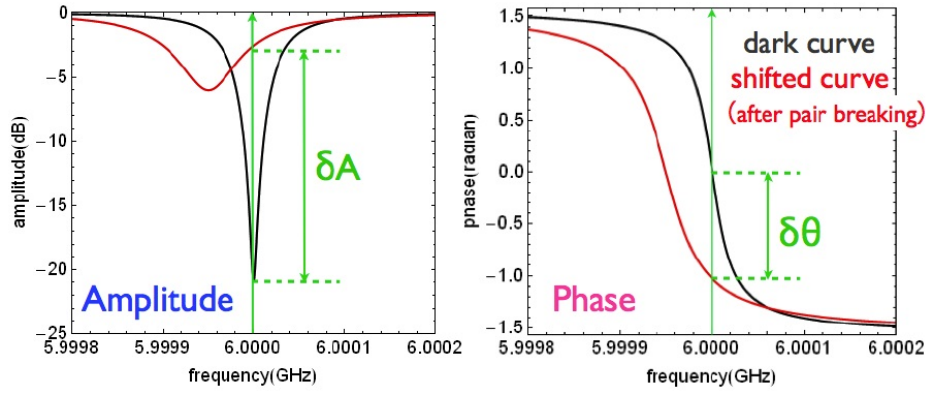


Figure 2.11: The variation of the S_{21} by the incident photon.

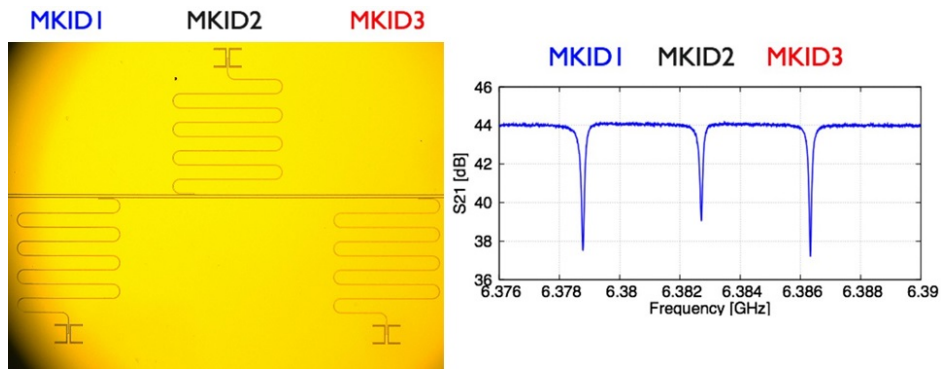


Figure 2.12: Frequency Domain Multiplexing of MKID.

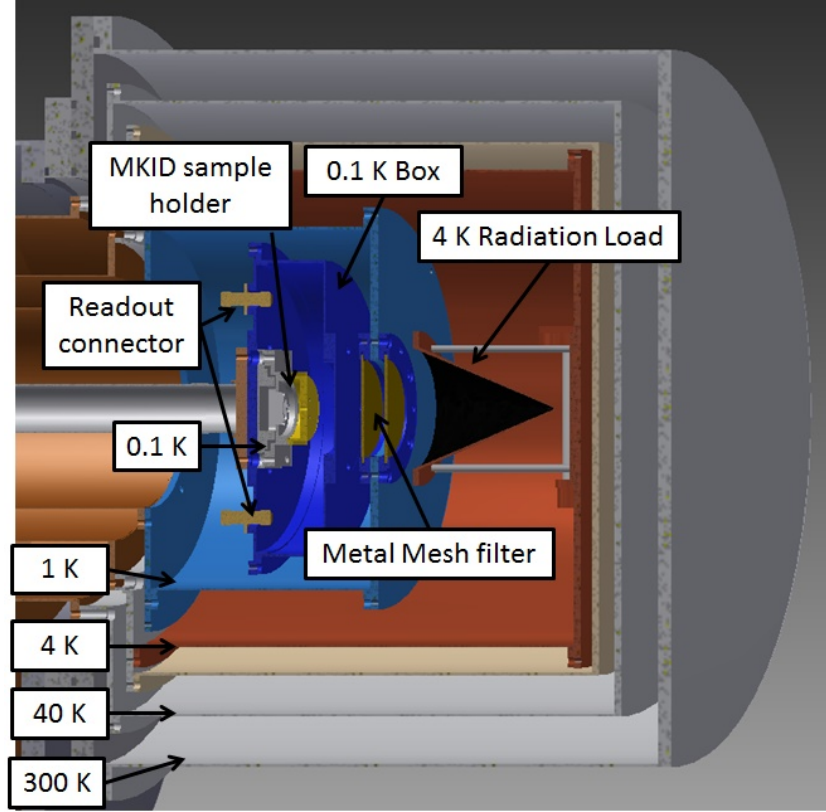


Figure 2.13: Light tight set up measurement system

decided by an excess noise. However, NEP_{Amp} depends on the Q strongly, and when an Al-MKID is used, the $Q = 4.5 \times 10^5$ and $NEP_{Amp} = 3 \times 10^{-18}$ W/\sqrt{Hz} have been reported [87].

The measured quality factor is Q_l including the whole resonator parts. Since Q_l has a relation with Q_i and Q_c via the eq.(2.19), high Q_i and Q_c are needed to make the Q_l higher. The coupler design defines the Q_c value. High Q_i should be get at lower temperature, however, the measured Q_i is saturated at the $T \sim T_c/10$. It is because the quasiparticles is generated by the incident stray light coming from the outside of the detector [88]. To reduce the stray light, a light tight setup has been designed [88][89].

Since the stray light, which has the energy above the gap one of the superconductor, generates the quasiparticles. In the case of an Al-MKID used in this thesis, the radiation above 90 GHz becomes the cause of the stray light. The main generation source of the stray light is the high temperature radiation shield. To reduce the stray light, the MKID is covered with the

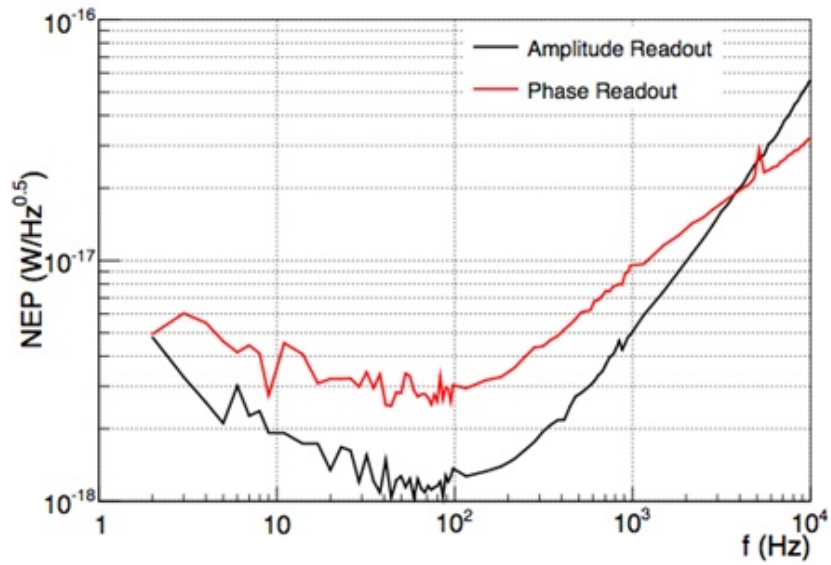


Figure 2.14: The NEP of an Al-MKID with the light tight set up[90].

double shields whose temperatures are the same as MKID (Fig. 2.13). The absorber coated inside of the shields absorbs the stray light. We have measured an Al-MKID NEP of 2×10^{-18} with this light tight setup (Fig. 2.14) [90].

Chapter 3

インターネット公表に関する使用承諾が雑誌社から得られないため本章については、非公開。

「Development of a Compact Cold Optics for Millimeter and Submillimeter Wave Observations」

IEEE Transactions on Terahertz Science and Technology 雑誌, 5 巻, 49-56 頁

Chapter 4

インターネット公表に関する使用承諾が雑誌社から得られないため本章については、非公開。

「Broadband Corrugated Horn Array with Direct Machined Fabrication」
IEEE Transactions on Terahertz Science and Technology 雑誌, 7 巻, 36-41 頁

Chapter 5

Summary

A wide field cryogenic re-imaging optics and broadband corrugated horn array have been developed. Summary of this thesis is in the following lists.

- Wide field compact cold optics
 - Scalable optical design, which consists of several optical modules, is promising for a focal plane array of a large single-dish telescope. The seven optical modules for the Antarctic 10 m terahertz telescope are designed to cover one-degree FoV focal plane.
 - High refractive index and low loss lenses are used for a compact optics. Silicon and alumina have high refractive index ($n = 3.4$ and 3.1) in millimeter wave at low temperature and it has advantages in condensation of light. Anti-reflection coating of these lenses using sub-wavelength structure and mixed epoxy has been developed.
 - To cooling down MKIDs to an appropriate temperature, three kinds of IR blocking filters are adopted. The IR blocking filters reduce infrared radiation sufficiently and have $\sim 78\%$ transmittance from 200 GHz to 250 GHz.
 - Reducing stray light is crucial to reduce the noise of MKIDs. A cold nested baffle has been developed to prevent the stray light into a focal plane. We simulated using the LightTools software that the baffle reduces by 74% of incident stray light.
 - The loading power of each pixel becomes large because of many IR blocking filters and the high temperature of the alumina lens. In the camera module design of the 10 m telescope, the loading power from the IR blocking filters and lenses has been reduced and the atmospheric emission becomes dominant.

- Broadband corrugated horn
 - A millimeter corrugated horn array has been developed. The beam shape is symmetry, the side lobe is less than -20 dB and the cross-polarization is less than -25 dB. The return loss is less than -15 dB in most design frequency bands.
 - Beam patterns of the horns were measured at room temperature and it is consistent with simulations. They have a few advantages of cutting of the weight and reduction of the reflection at the flat surface of the horn aperture plane of an array.
 - A corrugated horn coupled OMT-MKID is designed and demonstrated. In a cryogenic test with cold optics, hot (300 K) / cold (77 K) responses of MKID were confirmed. The horn-MKID has good polarization beam response and symmetric beam shape at 150 GHz.
 - Large focal plane camera modules using corrugated horn array have been designed for CMB B-mode polarization measurements. The modules cover the 55 - 330 GHz frequency range.

Table 5.1: Compliance matrix of the wide field compact optics and broadband corrugated horn

		Spec.	Result	
Compact	Coupling to telescope focus	F#/6	F#/6	
	Coupling to detector	F#/1	F#/1	
	Focal plane diameter (telescope)	100 mm	100 mm	
	Focal plane diameter (detector)	18.6 mm	18.6 mm	
Efficiency	IR filter in-band transmittance	> 80%	78%	
Loading	Loading Power of 1 pixel	< 15 pW	50 pW	220 GHz
Cooling	IR filter 10 μm transmittance	< 10^{-7}	< 10^{-9}	10 μm
	100 mK stage	< 3 μW	0.7 μW	91 mK
	4 K stage	< 1 W	529 mW	
	40 K stage	< 30 W	12.1 W	
Wide field	Field of View	1 deg	1 deg	Design
	Thermal power into 100 mK stage	< 20 μW	2.8 μW	Design
	Loading Power of 1 pixel	< 15 pW	13.6 pW	400 GHz
Corrugated horn	Bandwidth	> 1:2	1:2.25	
	Averaged return loss	< -15 dB	< -15 dB	
	Side-lobe level	< -20 dB	< -25 dB	
	Cross-polarization	< -20 dB	< -20 dB	

Bibliography

- [1] Planck Collaboration, R. Adam, P. Ade, N. Aghanim, Y. Akrami, M. Alves, F. Argüeso, M. Arnaud, F. Arroja, M. Ashdown, J. Aumont *et al.*, “Planck 2015 results-I. Overview of products and scientific results,” *Astron. Astrophys.*, vol. 594, 2016.
- [2] A. A. Penzias and R. W. Wilson, “A Measurement of Excess Antenna Temperature at 4080 Mc/s.” *Astrophys. J.*, vol. 142, pp. 419–421, 1965.
- [3] S. Dodelson, *Modern cosmology*, 2003.
- [4] J. C. Mather, E. Cheng, D. Cottingham, R. Eplee Jr, D. Fixsen, T. Hewagama, R. Isaacman, K. Jensen, S. Meyer, P. Noerdlinger *et al.*, “Measurement of the cosmic microwave background spectrum by the COBE FIRAS instrument,” *Astrophys. J.*, vol. 420, pp. 439–444, 1994.
- [5] K. Sato, “First-order phase transition of a vacuum and the expansion of the Universe,” *Monthly Notices of the Royal Astronomical Society*, vol. 195, pp. 467–479, 1981.
- [6] A. H. Guth, “Inflationary universe: A possible solution to the horizon and flatness problems,” *Phys. Rev. D*, vol. 23, pp. 347–356, Jan 1981.
- [7] H. Ishino, Y. Akiba, K. Arnold, D. Barron, J. Borrill, R. Chendra, Y. Chinone, S. Cho, A. Cukierman, T. de Haan *et al.*, “LiteBIRD: lite satellite for the study of B-mode polarization and inflation from cosmic microwave background radiation detection,” in *Proc. SPIE*, pp. 99 040X–99 040X, 2016.
- [8] M. Kamionkowski and E. D. Kovetz, “ The Quest for B Modes from Inflationary Gravitational Waves,” *Annu. Rev. Astron. Astrophys.*, pp. 227–269, 2016.
- [9] J. M. Kovac, E. Leitch, C. Pryke, J. Carlstrom, N. Halverson, and W. Holzappel, “Detection of polarization in the cosmic microwave background using *dasi*,” *Nature*, vol. 420, no. 6917, pp. 772–787, 2002.

- [10] M. Kamionkowski, A. Kosowsky, and A. Stebbins, “Statistics of cosmic microwave background polarization,” *Physical Review D*, vol. 55, no. 12, p. 7368, 1997.
- [11] M. Zaldarriaga and U. Seljak, “All-sky analysis of polarization in the microwave background,” *Physical Review D*, vol. 55, no. 4, p. 1830, 1997.
- [12] D. Hanson, S. Hoover, A. Crites, P. Ade, K. Aird, J. Austermann, J. Beall, A. Bender, B. Benson, L. Bleem *et al.*, “Detection of B-mode polarization in the cosmic microwave background with data from the south pole telescope,” *Phys. Rev. Lett.*, vol. 111, no. 14, p. 141301, 2013.
- [13] M. Hazumi, J. Borrill, Y. Chinone, M. Dobbs, H. Fuke, A. Ghribi, M. Hasegawa, K. Hattori, M. Hattori, W. Holzappel *et al.*, “LiteBIRD: a small satellite for the study of B-mode polarization and inflation from cosmic background radiation detection,” in *Proc. SPIE*, vol. 8442, p. 844219, 2012.
- [14] M. Tegmark, “CMB mapping experiments: a designer’s guide,” *Physical Review D*, vol. 56, no. 8, p. 4514, 1997.
- [15] Planck Collaboration, R. Adam, P. Ade, N. Aghanim, M. Arnaud, M. Ashdown, J. Aumont, C. Baccigalupi, A. Banday, R. Barreiro, N. Bartolo *et al.*, “Planck 2015 results - VII. High Frequency Instrument data processing: Time-ordered information and beams,” *Astron. Astrophys.*, vol. 594, 2016.
- [16] A. W. Blain, I. Smail, R. Ivison, J.-P. Kneib, and D. T. Frayer, “Submillimeter galaxies,” *Phys. Rep.*, vol. 369, no. 2, pp. 111–176, 2002.
- [17] C. M. Casey, C.-C. Chen, L. L. Cowie, A. J. Barger, P. Capak, O. Ilbert, M. Koss, N. Lee, E. Le Floch, D. B. Sanders *et al.*, “Characterization of Scuba-2 450 μm and 850 μm selected galaxies in the COSMOS field,” *Mon. Not. R. Astron. Soc.*, p. stt1673, 2013.
- [18] J. Vieira, D. P. Marrone, S. Chapman, C. De Breuck, Y. Hezaveh, A. Weiß, J. Aguirre, K. Aird, M. Aravena, M. Ashby *et al.*, “Dusty starburst galaxies in the early Universe as revealed by gravitational lensing,” *Nature*, vol. 495, no. 7441, pp. 344–347, 2013.
- [19] Y. Tamura, K. Kohno, K. Nakanishi, B. Hatsukade, D. Iono, G. W. Wilson, M. S. Yun, T. Takata, Y. Matsuda, T. Tosaki *et al.*, “Spatial

- correlation between submillimetre and Lyman- α galaxies in the SSA 22 protocluster,” *Nature*, vol. 459, no. 7243, pp. 61–63, 2009.
- [20] D. H. Hughes, S. Serjeant, J. Dunlop, M. Rowan-Robinson, A. Blain, R. G. Mann, R. Ivison, J. Peacock, A. Efstathiou, W. Gear *et al.*, “High-redshift star formation in the Hubble Deep Field revealed by a submillimetre-wavelength survey,” *Nature*, vol. 394, no. 6690, pp. 241–247, 1998.
- [21] E. Valiante, M. Smith, S. Eales, S. Maddox, E. Ibar, R. Hopwood, L. Dunne, P. Cigan, S. Dye, E. Pascale *et al.*, “The Herschel-ATLAS data release 1–I. Maps, catalogues and number counts,” *MNRAS*, vol. 462, no. 3, pp. 3146–3179, 2016.
- [22] S. Ishii, M. Seta, N. Nakai, S. Nagai, N. Miyagawa, A. Yamauchi, H. Motoyama, and M. Taguchi, “Site testing at Dome Fuji for submillimetre and terahertz astronomy: 220GHz atmospheric-transparency,” *Polar Sci.*, vol. 3, no. 4, pp. 213–221, 2010.
- [23] M. Seta, N. Nakai, S. Ishii, M. Nagai, Y. Miyamoto, T. Ichikawa, N. Takato, and H. Motoyama, “Dome Fuji in Antarctica as a Site for Infrared and Terahertz Astronomy,” *Proceedings of the International Astronomical Union*, vol. 8, no. S288, pp. 251–255, 2012.
- [24] J. E. Geach, E. L. Chapin, K. E. K. Coppin, J. S. Dunlop, M. Halpern, I. Smail, P. v. d. Werf, S. Serjeant, D. Farrah, I. Roseboom, T. Targett, V. Arumugam, V. Asboth, A. Blain, A. Chrysostomou, C. Clarke, R. J. Ivison, S. L. Jones, A. Karim, T. Mackenzie, R. Meijerink, M. J. Michaowski, D. Scott, J. M. Simpson, A. M. Swinbank, D. M. Alexander, O. Almaini, I. Aretxaga, P. Best, S. Chapman, D. L. Clements, C. Conselice, A. L. R. Danielson, S. Eales, A. C. Edge, A. G. Gibb, D. Hughes, T. Jenness, K. K. Knudsen, C. G. Lacey, G. Marsden, R. McMahon, S. J. Oliver, M. J. Page, J. A. Peacock, D. Rigopoulou, E. I. Robson, M. Spaans, J. Stevens, T. M. A. Webb, C. Willott, C. D. Wilson, and M. Zemcov, “The SCUBA-2 Cosmology Legacy Survey: blank-field number counts of 450- μ m-selected galaxies and their contribution to the cosmic infrared background,” *Monthly Notices of the Royal Astronomical Society*, vol. 432, no. 1, pp. 53–61, 2013. [Online]. Available: <http://mnras.oxfordjournals.org/content/432/1/53.abstract>
- [25] N. Kuno, H. Matsuo, Y. Mizumoto, A. Lange, J. Beeman, and E. Haller, “Seven matched bolometers for millimeter wave observa-

- tions,” *Int. J. Infrared and Millimeter Waves*, vol. 14, no. 4, pp. 749–762, 1993.
- [26] K. Irwin, “An application of electrothermal feedback for high resolution cryogenic particle detection,” *Appl. Phys. Lett.*, vol. 66, no. 15, pp. 1998–2000, 1995.
- [27] K. Irwin, G. Hilton, D. Wollman, and J. M. Martinis, “X-ray detection using a superconducting transition-edge sensor microcalorimeter with electrothermal feedback,” *Appl. Phys. Lett.*, vol. 69, no. 13, pp. 1945–1947, 1996.
- [28] P. K. Day, H. G. LeDuc, B. A. Mazin, A. Vayonakis, and J. Zmuidzinas, “A broadband superconducting detector suitable for use in large arrays,” *Nature*, vol. 425, no. 6960, pp. 817–821, 2003.
- [29] D. F. Filipovic, S. S. Gearhart, and G. M. Rebeiz, “Double-slot antennas on extended hemispherical and elliptical silicon dielectric lenses,” *IEEE Trans. Microw. Theory Tech.*, vol. 41, no. 10, pp. 1738–1749, 1993.
- [30] T. Nitta, K. Karatsu, Y. Sekimoto, M. Naruse, M. Sekine, S. Sekiguchi, H. Matsuo, T. Noguchi, K. Mitsui, N. Okada *et al.*, “Close-Packed Silicon Lens Antennas for Millimeter-Wave MKID Camera,” *J. Low Temp. Phys.*, vol. 176, pp. 684–690, 2014.
- [31] A. Suzuki, K. Arnold, J. Edwards, G. Engargiola, A. Ghribi, W. Holzapfel, A. T. Lee, X. F. Meng, M. J. Myers, R. O’Brien *et al.*, “Multi-chroic dual-polarization bolometric detectors for studies of the cosmic microwave background,” in *Proc. SPIE*, pp. 84 523H–84 523H, 2012.
- [32] K. Mitsui, T. Nitta, N. Okada, Y. Sekimoto, K. Karatsu, S. Sekiguchi, M. Sekine, and T. Noguchi, “Fabrication of 721-pixel silicon lens array of a microwave kinetic inductance detector camera,” *J. Astron. Telesc. Instrum. Syst.*, vol. 1, no. 2, pp. 025 001–025 001, 2015.
- [33] T. Nitta, S. Sekiguchi, Y. Sekimoto, K. Mitsui, N. Okada, K. Karatsu, M. Naruse, M. Sekine, H. Matsuo, T. Noguchi *et al.*, “Anti-reflection Coating for Cryogenic Silicon and Alumina Lenses in Millimeter-Wave Bands,” *J. Low Temp. Phys.*, vol. 176, pp. 677–683, 2014.

- [34] J. M. Edwards, R. O'Brient, A. T. Lee, and G. M. Rebeiz, "Dual-polarized sinuous antennas on extended hemispherical silicon lenses," *IEEE Trans. Antennas. Propag.*, vol. 60, no. 9, pp. 4082–4091, 2012.
- [35] X. Zhang, "Design of conical corrugated feed horns for wide-band high-frequency applications," *Microwave Theory and Techniques, IEEE Transactions on*, vol. 41, no. 8, pp. 1263–1274, 1993.
- [36] J. Teniente, R. Gonzalo, and C. Del-Rio, "Ultra-wide band corrugated gaussian profiled horn antenna design," *IEEE Microwave and Wireless Components Letters*, vol. 12, no. 1, pp. 20–21, jan 2002.
- [37] F. Takeda and T. Hashimoto, "Broadbanding of corrugated conical horns by means of the ring-loaded corrugated waveguide structure," *IEEE Trans. Antennas Propag.*, vol. 24, no. 6, pp. 786–792, 1976.
- [38] R. Datta, J. Hubmayr, C. Munson, J. Austermann, J. Beall, D. Becker, H.-M. Cho, N. Halverson, G. Hilton, K. Irwin *et al.*, "Horn coupled multichroic polarimeters for the Atacama Cosmology Telescope polarization experiment," *J. Low. Temp. Phys.*, vol. 176, no. 5, pp. 670–676, 2014.
- [39] G. Engargiola and R. L. Plambeck, "Tests of a planar L-band ortho-mode transducer in circular waveguide," *Review of Scientific Instruments*, vol. 74, no. 3, p. 1380, 2003.
- [40] J. McMahon, J. Beall, D. Becker, H. Cho, R. Datta, A. Fox, N. Halverson, J. Hubmayr, K. Irwin, J. Nibarger *et al.*, "Multi-chroic feed-horn coupled TES polarimeters," *J. Low. Temp. Phys.*, vol. 167, no. 5, pp. 879–884, 2012.
- [41] A. Olver, "Corrugated horns," *Electronics & Communication Engineering Journal*, vol. 4, no. 1, pp. 4–10, 1992.
- [42] Y. Béniguel, A. Berthon, C. V. Klooster, and L. Costes, "Design realization and measurements of a high performance wide-band corrugated horn," *IEEE Trans. Antennas Propag.*, vol. 53, no. 11, pp. 3540–3546, 2005.
- [43] K. Kimura, H. Iwashita, S. Asayama, M. Sugimoto, G. Kikuchi, and H. Ogawa, "Antenna performance of a directly dug corrugated feedhorn for the 150-GHz band," *Int. J. Infrared Millim. Waves*, vol. 29, no. 8, pp. 713–723, 2008.

- [44] J.-C. S. Chieh, B. Dick, S. Loui, and J. D. Rockway, "Development of a Ku-band corrugated conical horn using 3-D print technology," *IEEE Antennas Wirel. Propag. Lett.*, vol. 13, pp. 201–204, 2014.
- [45] S. Padin, "Mapping speed for an array of corrugated horns." *Applied optics*, vol. 49, no. 3, pp. 479–83, jan 2010.
- [46] R. W. Haas, D. Brest, H. Mueggenburg, L. Lang, and D. Heimlich, "Fabrication and performance of MMW and SMMW platelet horn arrays," *Int. J. Infrared Millim. Waves*, vol. 14, no. 11, pp. 2289–2293, 1993.
- [47] F. S. J. Mah and N. V. Shuley, "Design and construction of a highly efficient low cost wideband corrugated conical horn," in *RF and Microwave Conference, 2004. RFM 2004. Proceedings*, 2004, pp. 115–118.
- [48] J. Gundersen and E. Wollack, "Millimeter Wave Corrugated Platelet Feeds," in *Proc. J. Phys., Conf. Ser.*, vol. 155, p. 012005, 2009.
- [49] J. W. Britton, J. P. Nibarger, K. W. Yoon, J. A. Beall, D. Becker, H.-M. Cho, G. C. Hilton, J. Hubmayr, M. D. Niemack, and K. D. Irwin, "Corrugated silicon platelet feed horn array for CMB polarimetry at 150 GHz," in *Proc. SPIE*, vol. 7741, p. 77410T, 2010.
- [50] F. Del Torto, M. Bersanelli, F. Cavaliere, A. De Rosa, O. D'Arcangelo, C. Franceschet, M. Gervasi, A. Mennella, E. Pagana, A. Simonetto *et al.*, "W-band prototype of platelet feed-horn array for CMB polarisation measurements," *J. Instrum.*, vol. 6, no. 06, p. P06009, 2011.
- [51] L. Lucci, R. Nesti, G. Pelosi, and S. Selleri, "A Stackable Constant-Width Corrugated Horn Design for High-Performance and Low-Cost Feed Arrays at Millimeter Wavelengths," *IEEE Antennas Wirel. Propag. Lett.*, vol. 11, pp. 1162–1165, 2012.
- [52] J. Leech, B. K. Tan, G. Yassin, P. Kittara, S. Wangsuya, T. Boon Kok, G. Yassin, P. Kittara, and S. Wangsuya, "Experimental Investigation of a Low-Cost, High Performance Focal-Plane Horn Array," *IEEE Transactions on Terahertz Science and Technology*, vol. 2, no. 1, pp. 61–70, jan 2012.
- [53] M. I. Hollister, "The SCUBA-2 Instrument: An Application of Large-Format Superconducting Bolometer Arrays for Submillimetre Astronomy," Ph.D. dissertation, University of Edinburgh, 2009.

- [54] M. Calvo, A. Benoit, A. Catalano, J. Goupy, A. Monfardini, N. Pontthieu, E. Barria, G. Bres, M. Grollier, G. Garde *et al.*, “The NIKA2 instrument, a dual-band kilopixel KID array for millimetric astronomy,” *J. Low. Temp. Phys.*, pp. 1–8, 2016.
- [55] T. A. Sebring, R. Giovanelli, S. Radford, and J. Zmuidzinas, “Cornell Caltech Atacama Telescope (CCAT): a 25 m aperture telescope above 5000 m altitude,” in *Proc. SPIE*, vol. 6267, p. 62672C, 2006.
- [56] Nobeyama Radio Observatory HP. <http://www.nro.nao.ac.jp/en/index.html>.
- [57] H. Ezawa, R. Kawabe, K. Kohno, and S. Yamamoto, “The Atacama submillimeter telescope experiment (ASTE),” in *Proc. SPIE*, pp. 763–772, 2004.
- [58] Caltech Submillimeter Observatory HP. <http://cso.caltech.edu/>.
- [59] James Clerk Maxwell Telescope HP. <http://www.eaobservatory.org/jcmt/>.
- [60] J. Baars, B. Hooghoudt, P. Mezger, and M. de Jonge, “The IRAM 30-m millimeter radio telescope on Pico Veleta, Spain,” *Astron. Astrophys.*, vol. 175, pp. 319–326, 1987.
- [61] H. J. Kärcher and J. W. Baars, “Design of the large millimeter telescope/gran telescopio millimetrico (LMT/GTM),” in *Proc. SPIE*, pp. 155–168, 2000.
- [62] A. Kosowsky, “The Atacama Cosmology Telescope,” *New Astronomy Reviews*, vol. 47, no. 11, pp. 939–943, 2003.
- [63] Atacama Cosmology Telescope HP. <https://act.princeton.edu/>.
- [64] J. Ruhl, P. A. Ade, J. E. Carlstrom, H.-M. Cho, T. Crawford, M. Dobbs, C. H. Greer, W. L. Holzapfel, T. M. Lanting, A. T. Lee *et al.*, “The South Pole Telescope,” in *Proc. SPIE*, pp. 11–29, 2004.
- [65] K. Arnold, P. Ade, A. Anthony, F. Aubin, D. Boettger, J. Borrill, C. Cantalupo, M. Dobbs, J. Errard, D. Flanigan *et al.*, “The POLARBEAR CMB polarization experiment,” in *Proc. SPIE*, vol. 70, pp. 77 411E–77 411E, 2010.
- [66] Z. D. Kermish, P. Ade, A. Anthony, K. Arnold, D. Barron, D. Boettger, J. Borrill, S. Chapman, Y. Chinone, M. A. Dobbs *et al.*, “The POLARBEAR experiment,” in *Proc. SPIE*, vol. 8452, p. 84521C, 2012.

- [67] K. Yoon, P. Ade, D. Barkats, J. Battle, E. Bierman, J. Bock, J. Brevik, H. Chiang, A. Crites, C. Dowell *et al.*, “The Robinson Gravitational Wave Background Telescope (BICEP): a bolometric large angular scale CMB polarimeter,” in *Proc. SPIE*, vol. 6275, p. 62751K, 2006.
- [68] B. G. Keatinga, P. A. Adeb, J. J. Bocke, E. Hivond, W. L. Holzapfele, A. E. Langea, H. Nguyenb, and K. W. Yoon, “BICEP: a large angular scale CMB polarimeter,” in *Proc. SPIE*, vol. 4843, pp. 284–295, 2003.
- [69] P. Ade, R. Aikin, M. Amiri, D. Barkats, S. Benton, C. Bischoff, J. Bock, J. Brevik, I. Buder, E. Bullock *et al.*, “BICEP2 II: Experiment and Three-Year Data Set,” *Astrophys. J.*, vol. 792, p. 62, 2014.
- [70] J. E. Austermann, K. Aird, J. Beall, D. Becker, A. Bender, B. Benson, L. Bleem, J. Britton, J. Carlstrom, C. Chang *et al.*, “SPTpol: an instrument for CMB polarization measurements with the South Pole Telescope,” in *Proc. SPIE*, vol. 8452, p. 84521E, 2012.
- [71] R. Thornton, P. Ade, S. Aiola, F. Angile, M. Amiri, J. Beall, D. Becker, H. Cho, S. Choi, P. Corlies *et al.*, “The atacama cosmology telescope: The polarization-sensitive actpol instrument,” *Astrophys. J., Suppl. Ser.*, vol. 227, no. 2, 2016.
- [72] M. I. Hollister, N. G. Czakon, P. K. Day, T. P. Downes, R. Duan, J. Gao, J. Glenn, S. R. Golwala, H. G. LeDuc, P. R. Maloney *et al.*, “The cryomechanical design of MUSIC: a novel imaging instrument for millimeter-wave astrophysics at the Caltech Submillimeter Observatory,” in *Proc. SPIE*, vol. 7741, p. 77411L, 2010.
- [73] M. Hollister, N. Czakon, P. Day, R. Duan, J. Glenn, S. Golwala, H. Leduc, P. Maloney, B. Mazin, H. Nguyen *et al.*, “An Update on MUSIC: A Kinetic Inductance Detector Camera for Sub/Millimeter Astrophysics at the Caltech Submillimeter Observatory,” *Twenty-First International Symposium on Space Terahertz Technology*, vol. 1, pp. 263–269, 2010.
- [74] J. Sayers, N. G. Czakon, P. K. Day, T. P. Downes, R. P. Duan, J. Gao, J. Glenn, S. R. Golwala, M. I. Hollister, H. G. LeDuc *et al.*, “Optics for MUSIC: a new (sub) millimeter camera for the Caltech Submillimeter Observatory,” in *Proc. SPIE*.
- [75] R. Datta, C. Munson, M. Niemack, J. McMahon, J. Britton, E. J. Wollack, J. Beall, M. Devlin, J. Fowler, P. Gallardo *et al.*, “Large-aperture

- wide-bandwidth antireflection-coated silicon lenses for millimeter wavelengths,” *Applied optics*, vol. 52, no. 36, pp. 8747–8758, 2013.
- [76] P. J. B. Clarricoats and A. D. Olver, *Corrugated horns for microwave antennas*. IEE Electromagnetic Waves Series 18, 1984.
- [77] J. Zmuidzinas, “Superconducting microresonators: Physics and applications,” *Annu. Rev. Condens. Matter Phys.*, vol. 3, no. 1, pp. 169–214, 2012.
- [78] J. Bardeen, L. N. Cooper, and J. R. Schrieffer, “Theory of superconductivity,” *Physical Review*, vol. 108, no. 5, p. 1175, 1957.
- [79] T. Van Duzer and C. W. Turner, *Principles of superconductive devices and circuits*. Elsevier New York, 1981, vol. 31.
- [80] D. M. Pozar, *Microwave engineering*. Wiley.com, 2009.
- [81] B. A. Mazin, “Microwave Kinetic Inductance Detectors,” Ph.D. dissertation, California Institute of Technology, Pasadena, California, 2004.
- [82] F. Silsbee, R. Scott, J. Cook, and F. Brickwedde, “Superconductivity with Respect to Alternating Currents,” *Physical Review*, vol. 39, no. 2, p. 379, 1932.
- [83] J. McLennan, A. Burton, A. Pitt, and J. Wilhelm, “The Phenomena of Superconductivity with Alternating Currents of High Frequency,” *Proceedings of the Royal Society of London. Series A*, vol. 136, no. 829, pp. 52–76, 1932.
- [84] D. C. M. J. Bardeen, “Theory of the Anomalous Skin Effect in Normal and Superconducting Metals,” *Physical Review*, 1958.
- [85] J. Gao, “The Physics of Superconducting Microwave Resonators,” Ph.D. dissertation, California Institute of Technology, Pasadena, California, 2008.
- [86] R. Barends, “Photon-detecting superconducting resonators,” Ph.D. dissertation, Delft University of Technology, 2009.
- [87] J. Baselmans, S. Yates, R. Barends, Y. Lankwarden, J. Gao, H. Hovers, and T. Klapwijk, “Noise and sensitivity of aluminum kinetic inductance detectors for sub-mm astronomy,” *J. Low. Temp. Phys.*, vol. 151, no. 1-2, pp. 524–529, 2008.

- [88] R. Barends, J. Wenner, M. Lenander, Y. Chen, R. Bialczak, J. Kelly, E. Lucero, P. O'Malley, M. Mariantoni, D. Sank *et al.*, “Minimizing quasiparticle generation from stray infrared light in superconducting quantum circuits,” *Appl. Phys. Lett.*
- [89] J. Baselmans, S. Yates, P. Diener, and P. de Visser, “Ultra low background cryogenic test facility for far-infrared radiation detectors,” *J. Low. Temp. Phys.*, vol. 167, no. 3-4, pp. 360–366, 2012.
- [90] K. Karatsu, A. Dominjon, T. Fujino, T. Funaki, M. Hazumi, F. Irie, H. Ishino, Y. Kida, T. Matsumura, K. Mizukami *et al.*, “Radiation Tolerance of Aluminum Microwave Kinetic Inductance Detector,” *J. Low. Temp. Phys.*, pp. 1–7, 2016.
- [91] T. Nitta, “Development of the Wide-Field Camera System Using Kinetic Inductance Detectors for the Antarctic Terahertz Telescope,” Ph.D. dissertation, University of Tsukuba, 2014.
- [92] M. Naruse, Y. Sekimoto, T. Noguchi, A. Miyachi, K. Karatsu, T. Nitta, M. Sekine, Y. Uzawa, T. Taino, and H. Myoren, “Optical Efficiencies of Lens-Antenna Coupled Kinetic Inductance Detectors at 220 GHz,” *IEEE Trans. THz Sci. Technol.*, vol. 3, pp. 180–186, 2013.
- [93] ZEMAX, <https://www.zemax.com/home>.
- [94] CODE V, <http://optics.synopsys.com/codev/>.
- [95] M. Niemack, P. A. Ade, J. Aguirre, F. Barrientos, J. Beall, J. Bond, J. Britton, H. Cho, S. Das, M. Devlin *et al.*, “ACTPol: a polarization-sensitive receiver for the Atacama Cosmology Telescope,” in *Proc. SPIE*, vol. 7741, p. 77411S, 2010.
- [96] T. Matsumura, P. Ade, K. Arnold, D. Barron, J. Borrill, S. Chapman, Y. Chinone, M. Dobbs, J. Errard, G. Fabbian *et al.*, “POLARBEAR-2 optical and polarimeter designs,” in *Proc. SPIE*, vol. 8452, p. 84523E, 2012.
- [97] NIST HP. <http://cryogenics.nist.gov/index.htm>.
- [98] TAIYO NIPPON SANSO Co., <https://www.tn-sanso.co.jp/en/index.html>.
- [99] Sumitomo Heavy Industries Ltd., <http://www.shi.co.jp/english/index.html>.

- [100] P. Richards, “Bolometers for infrared and millimeter waves,” *J. Appl. Phys.*, vol. 76, no. 1, pp. 1–24, 1994.
- [101] T. Nitta, “Development of Camera Optics for the Antarctica Submillimeter Telescope,” Master’s thesis, Institute of Physics, University of Tsukuba, Tsukuba, Ibaraki, 305-8577, Japan, 2011.
- [102] J. Choi, H. Ishitsuka, S. Mima, S. Oguri, K. Takahashi, and O. Tajima, “Radio-transparent multi-layer insulation for radiowave receivers,” *Rev. Sci. Instrum.*, vol. 84, no. 11, p. 114502, 2013.
- [103] QMC Instruments Ltd. and Thomas Keating Ltd. HP. <http://www.terahertz.co.uk/>.
- [104] TYDEX HP. <http://www.tydex.ru>.
- [105] T. Nitta, M. Naruse, Y. Sekimoto, K. Mitsui, N. Okada, K. Karatsu, M. Sekine, H. Matsuo, T. Noguchi, Y. Uzawa *et al.*, “Beam Pattern Measurements of Millimeter-Wave Kinetic Inductance Detector Camera With Direct Machined Silicon Lens Array,” *IEEE Trans. THz Sci. Technol.*, vol. 3, pp. 56–62, 2013.
- [106] P. A. Ade, G. Pisano, C. Tucker, and S. Weaver, “A review of metal mesh filters,” in *Proc. SPIE*, vol. 6275, p. 62750U, 2006.
- [107] H. Matsuo, A. Sakamoto, and S. Matsushita, “FTS measurements of submillimeter-wave atmospheric opacity at Pampa la Bola,” *Publ. Astron. Soc. Japan*, vol. 50, no. 3, pp. 359–366, 1998.
- [108] D. J. Benford, M. C. Gaidis, and J. W. Kooi, “Optical properties of Zitex in the infrared to submillimeter,” *Appl. Opt.*, vol. 42, no. 25, pp. 5118–5122, 2003.
- [109] J. P. Emerson and W. Sutherland, “Visible and Infrared Survey Telescope for Astronomy- Overview,” in *Proc. SPIE*, vol. 4836, pp. 35–42, 2002.
- [110] I. Egan, E. Atad-Ettedgui, M. M. Casali, S. C. Craig, M. A. Ellis, P. R. Hastings, D. M. Henry, K. Laidlaw, J. Murray, M. Stewart *et al.*, “Vista IR camera: conceptual design,” in *Proc. SPIE*, vol. 4836, pp. 321–332, 2002.
- [111] LightTools, <http://optics.synopsys.com/lighttools/>.

- [112] M. Persky, “Review of black surfaces for space-borne infrared systems,” *Rev. Sci. Instrum.*, vol. 70, no. 5, pp. 2193–2217, 1999.
- [113] F. Pobell, *Matter and methods at low temperatures*. Springer, 1996, vol. 2.
- [114] C. Swenson, “Recommended values for the thermal expansivity of silicon from 0 to 1000 K,” *J. Phys. Chem. Ref. Data*, vol. 12, no. 2, pp. 179–182, 1983.
- [115] J. B. Wachtman, T. Scuderi, and G. Cleek, “Linear thermal expansion of aluminum oxide and thorium oxide from 100 to 1100 K,” *J. Am. Ceram. Soc.*, vol. 45, no. 7, pp. 319–323, 1962.
- [116] M. Sugimoto, Y. Sekimoto, S. Yokogawa, T. Okuda, T. Kamba, H. Ogawa, K. Kimura, T. Nishino, K. Noda, and K. Narasaki, “Thermal link for cartridge-type cryostat,” *Cryogenics*, vol. 43, no. 8, pp. 435–439, 2003.
- [117] K. E. Petersen, “Silicon as a mechanical material,” *Proc. IEEE*, vol. 70, no. 5, pp. 420–457, 1982.
- [118] T. Okada, “Operational Evaluation of a Multi-pixel Simultaneous Readout Circuite for Radio Astronomy Detectors,” Master’s thesis, The University of Tokyo, 2015.
- [119] H. Imada, “Theoretical Study of Radio Telescope Optics with Wide Field of View,” Ph.D. dissertation, University of Tsukuba, 2016.
- [120] M. Abbas-Azimi, F. Mazlumi, and F. Behnia, “Design of Broadband Constant-Beamwidth Conical Corrugated-Horn Antennas [Antenna Designer’s Notebook,” *IEEE Antennas and Propagation Magazine*, vol. 51, no. 5, pp. 109–114, oct 2009.
- [121] S. Shu, S. Sekiguchi, M. Sekine, Y. Sekimoto, T. Nitta, A. Dominjon, T. Noguchi, M. Naruse, and W. Shan, “Development of octave-band planar ortho-mode transducer with kinetic inductance detector for Lite-BIRD,” in *Proc. SPIE*, vol. 9914, p. 99142C, 2016.
- [122] Y. Sekimoto, S. Sekiguchi, S. Shu, M. Sekine, T. Nitta, M. Naruse, A. Dominjon, T. Hasebe, W. Shan, T. Noguchi *et al.*, “Design of corrugated-horn-coupled MKID focal plane for CMB B-mode polarization,” in *Proc. SPIE*, vol. 9914, p. 99142A, 2016.

- [123] P. F. Goldsmith, *Quasioptical systems: Gaussian beam quasioptical propagation and applications*. IEEE Press., 1998.
- [124] J. P. Nibarger, J. A. Beall, D. Becker, J. Britton, H.-M. Cho, A. Fox, G. C. Hilton, J. Hubmayr, D. Li, J. McMahon *et al.*, “An 84 pixel all-silicon corrugated feedhorn for CMB measurements,” *J. Low. Temp. Phys.*, vol. 167, no. 3, pp. 522–527, 2012.
- [125] L. Zeng, C.-y. E. Tong, E. J. Wollack, and D. T. Chuss, “A wideband profiled corrugated horn for multichroic applications,” in *2015 40th International Conference on Infrared, Millimeter, and Terahertz waves (IRMMW-THz)*. IEEE, 2015, pp. 1–2.
- [126] V. Tapia, R. Nesti, A. González, I. Barrueto, F. Mena, N. Reyes, F. Villa, F. Cuttaia, and P. Yagoubov, “An ultra-broadband optical system for ALMA Band 2+3,” in *Proc. SPIE*, vol. 9914, p. 99142X, 2016.
- [127] S. Shu, “Development of superconducting MKID camera for CMB B-mode polarization,” Master’s thesis, The University of Tokyo, 2015.
- [128] Virginia Diodes Inc. <http://www.vadiodes.com/en/>.